CHALMERS

Hydrocarbon Activation for Lean NO$_x$ Reduction over Ag-alumina

Master of Science Thesis

SEYYEDMAJID SHARIFVAGHEFI

Department of Chemical and Biological Engineering
Division of Applied Surface Chemistry
Competence Center for Catalysis
CHALMERS UNIVERSITY OF TECHNOLOGY
Göteborg, Sweden, 2011

Hydrocarbon Activation for Lean NOₓ Reduction over Ag-alumina

Seyyedmajid Sharifvaghefi

A master thesis performed at:
Competence Centre for Catalysis

CHALMERS UNIVERSTY OF TECHNOLOGY

Göteborg, 2011

Supervisors: Associate Professor Hanna Härelind Ingelsten, Competence Center for Catalysis and Applied Surface Chemistry
Associate Professor Per-Anders Carlsson, Competence Center for Catalysis and Applied Surface Chemistry

Examiner: Professor Magnus Skoglundh, Competence Center for Catalysis and Applied Surface Chemistry

Abstract

The reduction of nitrogen oxides, NO_x, with three different C_2 hydrocarbons (C_2H_2, C_2H_4, C_2H_6) under lean conditions (HC-SCR) over two set of silver alumina catalysts with 2 and 6% silver content was investigated. Surface area and pore size distribution of the prepared samples were measured and determined according to the BET and BJH methods. The catalytic properties of the samples were then investigated in flow reactor experiments using gas-phase FTIR. Formed surface species over catalysts with C_2H_2 and C_2H_4 as reductants, were further studied by DRIFTS in step-response experiments. The flow reactor experiments show that C_2H_2 has the lowest activation temperature and results in highest NO_x conversion with widest temperature window among the different C_2 hydrocarbons. C_2H_4 is activated at lower temperature than C_2H_6, however, the highest NO_x reduction reached with C_2H_6 was higher than for C_2H_4. The temperatures corresponding to the highest NO_x conversions were lower for reactions over the catalyst with highest silver content which shows higher oxidation ability of the catalyst with 6% Ag loading compared to the catalyst with 2% silver loading. The DRIFTS experiments show higher impact of reducing agent compared to the silver content on the NO_x reduction. Furthermore, different reaction pathway for NO_x reduction with C_2H_2 and C_2H_4 hydrocarbons as reductants is suggested.

Table of Contents

1. Introduction

1.1 Background

Since the industrial revolution, human activities have caused considerable environmental impact that has led to changes of the earth's climate [1, 2]. One aspect of the climate changes is global warming, which is the increase in average temperature of the atmosphere and oceans. During the 20th century, an increase of mean temperature of earth surface of approximately 0.4-0.8 °C has been measured. Although the consequences of global warming are not completely known, increase of sea level, melting glaciers, alters in the distribution of plants and animals and growing length of seasons are considered to be some of the negative effects [2, 3]. One of the known main causes for global warming is the increased amount of green house gases, mainly carbon dioxide but also hydrocarbons and nitrogen oxides, in the atmosphere through the burning of fossil fuels [1, 2]. Besides global warming, these gases cause other environmental and health problems as well. For example, nitrogen oxides are considered to give rise to acidic rain, the formation of photochemical smog and secondary particulate matter, and have harmful effects on breathing functionality and the cardio-circulatory system in humans [4, 5]. These problems have caused a great aspiration to control the concentration of green-house gases in the atmosphere, which has lead towards several legislations. Among all legislations initiated by United Nations, the "Framework Convention" in 1992, "Kyoto Protocol" in 1997 and the most recent one "Panel on Climate Change" in 2007 are considered to be the most important [6, 7, 8].

Today, almost 90% of the consumed energy origins from fossil fuels, of which nearly 60% is supplied via oil and natural gas [9]. Within the transportation sector, oil and associated derivatives dominates, *cf.* Fig. 1.a, and specifically road transports counts for about 80% of energy consumption, see Fig. 1.b [1]. All types of transportation, with only a few exceptions, emit air pollutants. Basically, unburned or partially burned hydrocarbons (HC), carbon monoxide (CO) and nitrogen oxides (NO_X) are the result of imperfect combustion and/or high combustion temperature in the combustion chamber [10, 11]. Thus transportation is a major source of air pollution, especially in urban areas, including green house gases and therefore a key aspect in all mentioned legislations [1, 12]. Consequently, there have been many efforts for improving both the emission control as well as fuel economy for both gasoline and diesel engines [6].

Diesel engines are generally more fuel-efficient than gasoline engines because of the higher air-to-fuel ratio (A/F > 14) as compared to stoichiometric gasoline engines. Moreover, the necessary endurance of the catalyst used for controlling the emissions from diesel engines are often more easily met than for gasoline engines as the (highest) exhaust temperatures are usually lower (≤800–850 °C) compared to the stoichiometric engines (up to 1100 °C) [10].
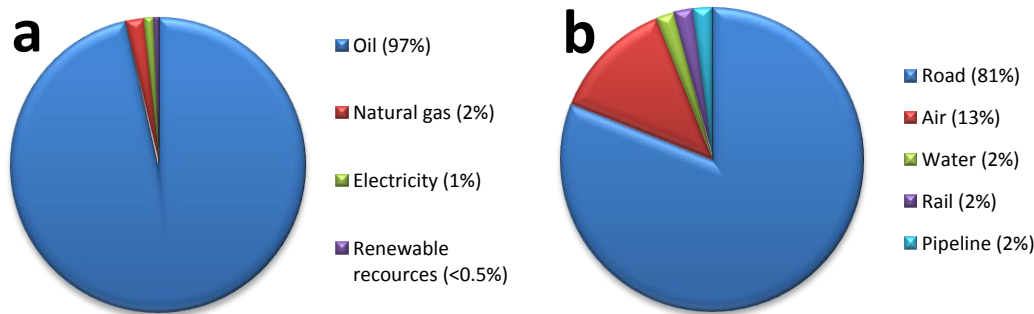
Fig. 1. Fuel use in the transportation sector in OECD (Organization for Economic Cooperation) [1].

Although diesel engines have become increasingly popular, for the mentioned reasons, the emission control from diesel engines is more difficult. This is due to the fact that diesel engines operate with a large excess of air leading to a considerable concentration of oxygen in exhausts, which makes reduction of NO_X emissions difficult [6, 13]. The oxygen concentration in typical diesel exhausts is usually between 10 and 14% while in gasoline exhausts the oxygen concentrations is controlled to be below 1%. This is a result of the operational window for the conventional three-way catalyst (TWC) used for emission control for gasoline vehicles. The TWC simultaneously converts NO_x, hydrocarbons and CO, and the conversion efficiency for all the components is 80% and above, for the air-to-fuel ratios defined by the operational window. However, the TWC is easily deactivated even in an atmosphere with an oxygen content of 2–3% at moderate temperatures by oxidative poisoning of the Rh and Pd metals [4]. Another problem with TWC catalysts in lean exhaust conditions is that the availability of the excess oxygen in the exhaust makes oxidation reactions (given below) more favorable than reduction reactions, so most of CO and hydrocarbons needed for reduction of NO react with oxygen to form CO_2 and H_2O. The reaction steps and operating window in a typical TWC are shown below [14].

Oxidation:

$$C_yH_n + \left(1 + \frac{n}{4}\right)O_2 \rightarrow yCO_2 + \frac{n}{2}H_2O$$

$$CO + \frac{1}{2}O_2 \rightarrow CO_2$$

$$CO + H_2O \rightarrow CO_2 + H_2$$

$$NO + \frac{1}{2}O_2 \rightarrow NO_2$$
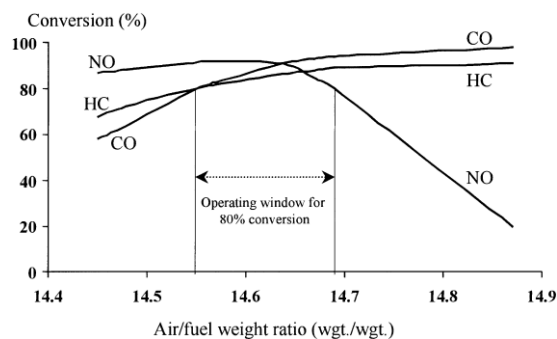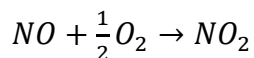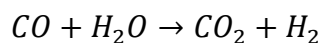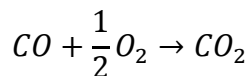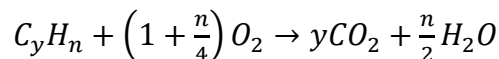
Fig. 2. Three way catalyst performance determined by engine air to fuel ratio [14].

7

Reduction:

$$NO\,(or\;NO_2) + CO \rightarrow \frac{1}{2}N_2 + CO_2$$

$$NO\,(or\;NO_2) + H_2 \rightarrow \frac{1}{2}N_2 + H_2O$$

$$\left(2 + \frac{n}{2}\right)NO\,(or\;NO_2) + C_yH_n \rightarrow \left(1 + \frac{1}{4}\right)N_2 + yCO_2 + \frac{n}{2}H_2O$$
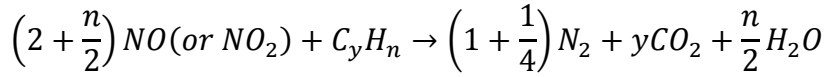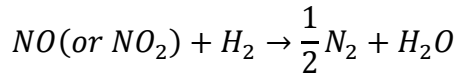
Recently, efforts have been made to substitute stoichiometric gasoline engines with engines operating with excess air, so-called lean-burn gasoline engines, because of their higher fuel efficiency, typically about 15% improvement. However, as with the diesel engine, lean-burn gasoline engines produce emissions for which the oxygen concentration is significant so the same problem arises for reduction of nitrogen oxides. It is scientifically challenging to reduce nitrogen oxides under strongly oxidizing conditions [6].

1.2 Objectives

The objective of this work is to investigate how the oxidizing ability of the silver-alumina HC-SCR catalyst is influenced by the silver loading (2% and 6% Ag). Three different C_2 hydrocarbons (C_2H_2, C_2H_4 and C_2H_6) were used to study how the C-C bond type influences the oxidation of the hydrocarbons and the formation of oxygenated intermediates and products. Furthermore, the selective catalytic reduction of NO_X is also studied, using the above mentioned hydrocarbons as reducing agents. This enables comparison of the oxidizing and reducing ability of the catalysts and considering reaction intermediates and products.

2. Catalytic NO$_X$ reduction

2.1 NO$_X$ removal technologies for vehicles

Currently there are several technologies for removal of NO$_X$ from vehicle exhausts. Each of these technologies is associated with advantages and disadvantages. The most important technologies are briefly described below.

2.1.1 Catalytic direct decomposition of NO

The ideal solution for catalytic reduction of NO$_X$ is to find a catalyst capable of decomposing NO directly in one step:

$$NO \rightarrow N_2 + O_2$$
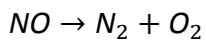
This technique is attractive, as no reducing agent is needed. The fact that the products N$_2$ and O$_2$ are thermodynamically more stable than the reactant NO makes this method promising. However, hitherto suitable catalysts have not yet been formulated especially catalysts that are active for NO$_X$ removal at realistic conditions [14, 15, 16].

2.1.2 Exhaust gas recirculation (EGR)

Exhaust gas recirculation (EGR) is a method where part of the exhaust gas is fed back into the engine (recirculation) in order to lower the flame temperature and the oxygen concentration in the combustion chamber, which are two of the main reasons for NO$_X$ formation. A drawback is that EGR increases the emission of particulate matter (PM) because of the lower oxygen concentration in the combustion chamber [16, 17].

2.1.3 Selective NO$_X$ recirculation (SNR)

The concept of selective NO$_X$ recirculation (SNR) is based on a two-step process where first NO$_X$ is adsorbed by a sorbent with high NO$_X$ selectivity and then desorbed (at higher temperature) and recirculated back into the combustion chamber where the combustion processes contribute to NO$_X$ reduction [18].

2.1.4 NO$_X$ storage- and reduction (NSR) catalysis

In the NO$_X$ storage- and reduction concept the catalyst is operated alternatively between lean and rich conditions. Under lean conditions (minutes), exhaust NO is oxidized to NO$_2$ over precious metals and then stored in the form of nitrate ions on the storage sites. Thereafter, under rich conditions (seconds), the nitrate ions are released as NO$_X$ and subsequently reduced to N$_2$ by a reducing agent such as H$_2$, CO and HC, *cf.* Fig. 3. A NSR catalyst usually contains precious metals, such as Pt or Pd and Rh, a support with high surface area, such as alumina, and alkaline or alkaline earth metal oxides as storage component, like barium and barium oxide [19, 20].
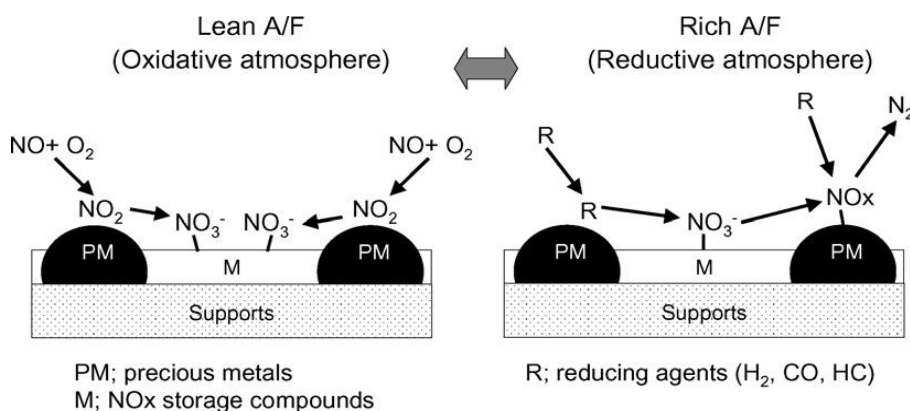
Fig. 3. Schematic view of NSR method [19].

2.1.5 Selective catalytic reduction of NO_x with ammonia

The selective catalytic reduction (SCR) of NO_X with ammonia (NH_3) was first discovered in 1957 [21]. The development of this technology was mainly aimed for NO_X reduction in stationary application such as boilers, incinerators and power plants [22]. It was shown that ammonia is able to selectively react with NO_x to form N_2 over Pt catalyst in excess of oxygen. The major desirable reactions for this process are [21]:

$$4NH_3 + 4NO + O_2 \rightarrow 4N_2 + 6H_2O$$

$$4NH_3 + 4NO_2 + O_2 \rightarrow 3N_2 + 6H_2O$$
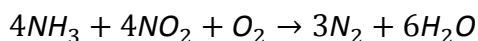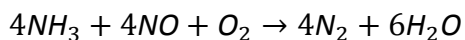
There are also undesirable reactions, which can take place simultaneously as the ones above. Two such side reactions are:

$$2NH_3 + 2O_2 \rightarrow N_2O + 3H_2O$$

$$4NH_3 + 3O_2 \rightarrow N_2 + 6H_2O$$
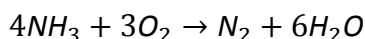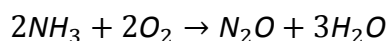
Later studies showed that Pt may lead to poor selectivity for NO_X reduction at temperatures above 250°C. Thus attention was paid to find more suitable catalysts capable of working at higher temperatures. Base metals and their oxides, e.g., V_2O_5-WO_3-TiO_2, rendered interest for exhaust gas cleaning at higher temperatures. Also, zeolite based catalysts were developed which could operate at higher temperatures compared to the previous catalysts. Fig. 4 shows the difference in operating temperatures for these types of materials [21].
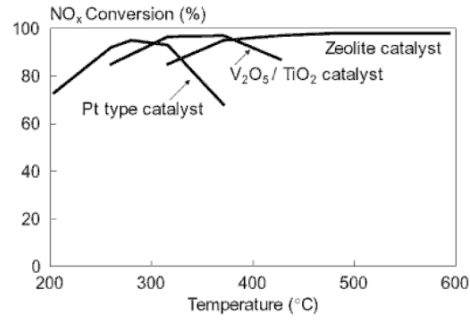
Fig. 4. Operating temperature for different SCR catalysts [21].

One of the first publications describing a SCR system for automotive usage was by Held *et al.* [23] in 1990. They showed that NO_X reduction from diesel exhausts under oxidizing conditions is improved by adding a substance containing urea as a reducing agent. In this process urea is used as a liquid carrier for ammonia, which decomposes to ammonia and carbon monoxide after injection to hot exhaust gas. The produced ammonia is then used to reduce NO_X in the exhaust gas. Some of the major problems with this method are: need for urea refueling infrastructure, installing extra diagnostic instruments to control injection and ammonia slip [14, 24]. The layout of a vehicle with this system is shown below (Figure 5).
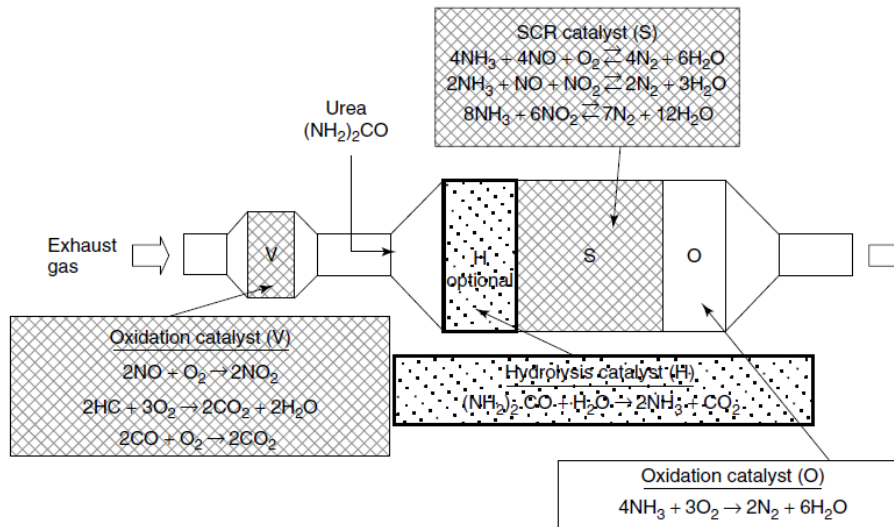
Fig. 5. Layout of a modern SCR-catalyst system (VHSO system with V: oxidation catalyst dedicated for NO2 generation; H: hydrolysis catalyst; S: selective reduction catalyst and O: oxidation catalyst dedicated for NH3 removal) [25].

2.1.6 Combined NSR and SCR

Recently, attention has been paid studying the ability of combining a NSR system with an ammonia-SCR system (or a physical mixture of these catalysts) for NO_X reduction. It is shown that using a CuZSM-5 based NH_3-SCR catalyst downstream of the NSR catalyst can increase the efficiency of NO_X removal compared to just using NSR. The ammonia formed on the NSR catalyst in rich periods is used as reducing agent in the SCR. It is also shown that the mixture of Pt–Rh/Ba/Al_2O_3 + Cu/ZSM-5 improves the NO_X reduction compared to NSR alone. Addition of water in the gas phase resulted in a reduction in activity of the catalyst, however the activity of the mixed catalysts was still higher than for NSR alone [26, 27].

2.2 Selective catalytic reduction of NO_X with hydrocarbons (HC-SCR)

The selective catalytic reduction of NO_x can also be based on catalysts that can convert NO_X through reaction with hydrocarbons or alcohols (HC-SCR) instead of ammonia. Typical reactions are [25]:

$$(6m + 2)NO + 2C_mH_{2m+2} \leftrightarrow (3m + 1)N_2 + 2mCO_2 + (2m + 2)H_2O$$

$$6mNO + 2C_mH_{2m+1}OH \leftrightarrow 3mN_2 + 2mCO_2 + (2m + 2)H_2O$$
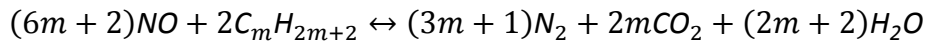
Reduction of NO through HC-SCR in oxidizing atmosphere was independently reported for Cu/ZSM-5 catalysts by Iwamato *et al.* and Hamada *et al.* [28]. Since then, development of this technique has been under intensive investigations. Further studies show that Cu/ZSM-5 is not a suitable catalyst for the HC-SCR process in realistic exhaust conditions mainly due to fast deactivation when exposed to sulfur (originating from the fuel or the engine oil), poor hydrothermal stability in the diesel exhaust and inhibiting effects of water [29, 30]. Later works by Hamada *et al.* [31] and Obuchi *et al.* [32] demonstrated the effectiveness of platinum group metals for HC-SCR particularly at low temperatures (i.e. 200-350 °C). Studies also show that Pt-based catalysts are resistant to water and SO_X poisoning and they have high hydrothermal stability [29, 33]. However, two main drawbacks are identified for these catalysts, i.e. very narrow temperature window for NO reduction due to oxidation of the reducing agent (i.e. hydrocarbon) by oxygen at higher temperatures, and the considerable formation of N_2O (i.e. low selectivity for N_2 formation) [34].

To conclude, the main advantage of the HC-SCR process is that no storage tank for reductant is needed and the fuel itself can be used as the reducing agent. However the HC-SCR technology is still not mature enough to be used for the NO_X abatement in vehicles equipped with diesel engines. More research is needed to find efficient NO_X removal catalysts for lean engines using on-board derived hydrocarbons as reductant giving conversions higher than 80%. Finding a solution to this problem will be a challenge in the future and a solution will represent a major breakthrough in NO_X reduction technology in automotive industry.
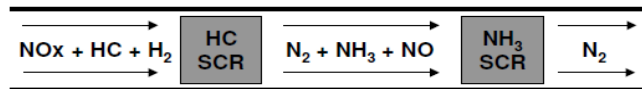
Fig. 6. Dual SCR Concept [35].

2.2.1 Dual SCR system

In a study by Fisher *et al.* [35], it is claimed that utilizing a dual SCR system they were able to obtain NO_X reduction efficiencies greater than 90% under lean conditions without the usage of precious metals or urea injection. As shown in Fig. 6 their dual SCR system contained an HC-SCR (silver-alumina) catalyst followed by an NH_3-SCR (Fe based zeolite) catalyst. It is suggested that NO_X reacts with hydrocarbons and hydrogen over the HC-SCR catalyst and mainly forms nitrogen and sufficient amount of ammonia, which reacts with unreacted NO_x over the NH_3-SCR catalyst to improving the NO_x reduction performance of the system.

2.3 The Ag/Al_2O_3 system

2.3.1 General aspects

One of the most promising candidates for the HC-SCR process is the silver alumina catalyst (Ag/Al_2O_3) which has shown high activities for NO_X reduction by hydrocarbons in the presence of water and excess oxygen and has moderate tolerance to water and SO_2 [36, 37]. Studies have shown high activity of the silver alumina catalyst for NO_X reduction with a wide range of hydrocarbons, such as light hydrocarbons [38], heavy hydrocarbons [33] and oxygenated hydrocarbons [36]. In 2000, studies by Shimizu *et al.* [33] showed that NO_X removal activity and water tolerance of Ag/Al_2O_3 were noticeably increased with increasing carbon number of the alkane reductants. Furthermore, the authors showed that among different transition metals supported on alumina, silver has the highest NO conversion using n-octane as reductant, *cf.* Fig. 7. However one important drawback of this system is the poor activity at low exhaust gas temperatures. Even though increasing the hydrocarbon chain length significantly improves the low temperature activity, this is not sufficient for a real application. Adding hydrogen to the exhaust gas significantly increases the low temperature activity in the HC-SCR reaction. The effect of hydrogen on NO_x reduction over Ag/Al_2O_3 under lean conditions was first identified by Satokawa [39]. He showed that the NO reduction activity by C_3H_8 at low temperature (590-760 K) is significantly increased by adding H_2 in presence of excess oxygen and water vapor.
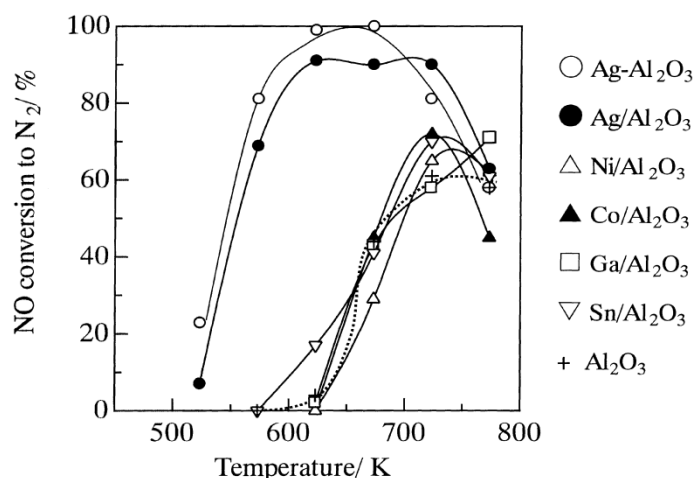
Fig. 7. Comparison of the catalytic activity of various alumina-supported metal oxide catalysts (M/Al2O3) and Ag–Al2O3 for SCR by n–octane. Conditions: NO=1000 ppm, HC=6000 ppm C, O_2=10%, H_2O=2%, W/F=0.12 g.s.cm^{-3} [35].

The exact mechanism of hydrogen effect is still under debate and there are different suggestions in the literature. One is that cyanide conversion to isocyanate is the rate-determining step and hydrogen is suggested to promote this conversion. Another is that hydrogen reduces surface nitrates to the more reactive nitrite species, which then reacts further with the hydrocarbon reductant. Disagreement of the role of hydrogen may be caused by different experimental conditions in the various studies. It is possible that all these promotional effects are important but the overall impact of them is dependable on the reaction temperature and gas composition [40, 41].

2.3.2 Synthesis of small silver species and model silver-alumina catalysts

The role of the state of Ag species in Ag/Al_2O_3 catalysts for NO_X reduction in lean conditions has been the subject of many studies. It is shown that different forms of the oxidized silver like Ag$^+$, Ag_2O or silver aluminate favors the reduction of NO to N_2 [42, 43, 44, 45], while metallic silver particles are more active for oxidation reaction of NO to NO_2 [46, 47, 48]. It is also suggested that Ag$_n^{\delta+}$ clusters are highly active species for HC-SCR [49] and they can activate the reducing agent by partial oxidation [50]. These findings indicate that catalyst samples which are active for NO_X reduction most likely contain highly dispersed ionic, oxidized and/or Ag$_n^{\delta+}$ silver species. Fig. 8 shows the different state of Ag species and their role in HC-SCR.
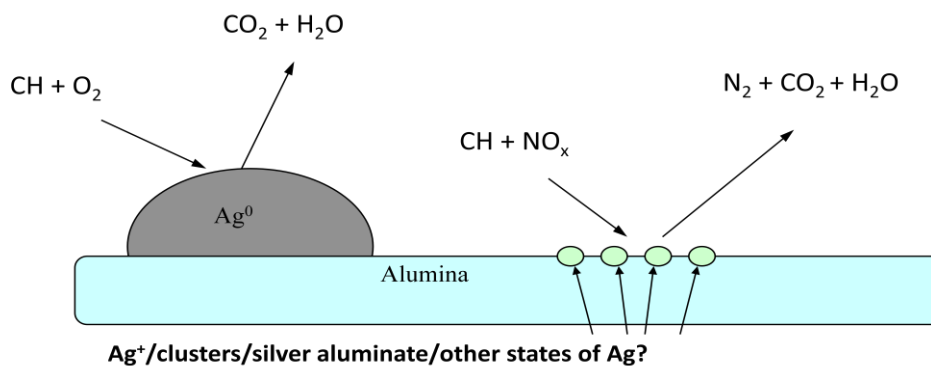
Fig. 8. State of Ag species and their role in HC-SCR

Sol–gel syntheses are generally known for the versatility, which allows better control of the texture, composition, homogeneity and structural properties of the produced catalysts [51]. Moreover, in a recent study by Kannisto *et al.* [52], it is shown that prepared samples of silver-alumina catalyst by the sol-gel method contain higher quantity and dispersion of non-metallic silver, i.e. clusters and/or oxidized silver species compared to the prepared samples by impregnation method. The authors also show that by implementing the 'freeze dried' sol-gel method for preparation of the samples a higher dispersion of silver is achieved compared to the thermally dried sol-gel samples. This is mainly owing to the fact that using freeze drying instead of thermal drying, has the advantage of avoiding the destructive effect of capillary pressure associated with the liquid-vapor interface within a pore. In freeze-drying sublimation of water inhibits the transformation of water into the liquid phase [53]. Therefore, this method helps to preserve the highly porous structure of the catalyst and also to maintain high dispersion of silver on the alumina support.

In order to evaluate catalysts in flow reactor experiments with more realistic conditions, like high space velocities, the powder samples can be coated onto monolith substrates. This is also what is done within automotive industry in order to get a durable structure and low pressure drop for the catalyst. The ceramic monolith used in this work had 400 cells per square inch, diameter of 20 mm and height of 21 mm. The advantage of using a monolith with higher cell density is the higher effectiveness of catalysts because of providing higher available surface area for catalysts' distribution. However, washcoating of these monoliths is harder and also they cause higher pressure drop [54].

15

3. Experimental section

3.1 Catalyst preparation and characterization

3.1.1 Preparation of Ag/Al₂O₃ powder

Based on the facts mentioned in the previous chapter, the "freeze dried sol-gel" method was selected for catalyst preparation in this study.

The process of forming sol-gel involves two steps, the formation of a sol and then formation of a gel. A sol is a colloidal suspension of solid particles in a liquid ranging in size from 1 nm to 1 micron. In a colloidal suspension the particles of the dispersed phase are so small that the effect of gravitational forces is very weak and interactions are prevailed by short range forces, such as van der Waals attraction and surface charges. The small enough inertia of dispersed particles causes a random walk when the particles collide with the suspending medium's molecules. This effect is called the Brownian motion and is the main reason that keeps particles suspended in the liquid phase. The sol can be prepared by hydrolysis followed by condensation of a precursor which can be an inorganic salt or a metal alkoxide. Metal alkoxides are popular precursors because they easily react with water and this has caused the widely usage of them in sol-gel research. The further condensation of sol particles can link hydrolyzed molecules until it forms a three-dimensional network called gel with the solid phase encapsulating the solvent. In this work the selected precursor for alumina was AIP (Aluminum Isopropoxide) which is a metal alkoxide. Silver nitrate ($AgNO_3$) was used as the silver precursor. The hydrolysis and condensation reactions for these precursors are as follows [53, 55]:

$AIP[Al(OR_3)] + 3H_2O \leftrightarrow Al(OH)_3 + 3ROH$ (Hydrolysis- Restrefication)

$Al(OH)_3 + Al(OH)_3 \leftrightarrow Al_2O_3 + 6H_2O$ (Water condensation- Hydrolysis)
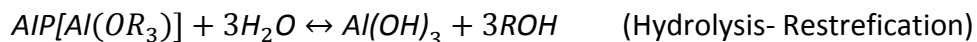
In a SCR study by n-octane, it is illustrated that in a low temperature region (573–623 K), 2% silver laoding provides the highest NO reduction among different Ag loadings [37]. Based on this fact , two different sets of catalysts (to enable us for later comparison) with 2% (F2) and 6% Ag (F6) loading was prepared by the following steps.

First AIP was dissolved in milli-Q water and the solution was mixed at 400 rpm using a magnetic stirrer. After that the silver nitrate was added to the solution while it was kept under stirring. The slurry was then heated to 82°C. In the next step, nitric acid (10%), was added to the slurry until it was cleared, and a sol was formed. The sol was then stirred at the mentioned temperature for 12 hours and thereafter it was heated in a water bath under vacuum (to remove the condensed water) until the gel was formed. Finally the remains of water were removed by freeze drying under vacuum. The precursors and their used amount for preparation of the powder catalyst samples are shown in Table 1.

Table 1: measured amount of precursors used for powder catalyst preparation.

Sample	Nominal Ag content [wt%] in Ag/Al_2O_3	AIP [gr]	$AgNO_3$ [gr]
F2	2	19.633	0.160
F6	6	18.847	0.471

3.1.2 Preparation of monolith catalysts

The usual method to attach the catalyst onto the monoliths is washcoating. By dipping the monolith structure into a slurry solution containing the catalyst and then heat treating, i.e. to calcine the monolith at high temperature, the monolith is coated with the catalyst. Using high temperatures to bind the catalyst to the monolith can cause sintering of the active phase as well as the support therefore, it is more suitable to use a binding material although the binder to some extent can cover the active phase and may block pores in the support material. To overcome this problem, the amount of binder used should be as low as possible [54, 56]. The binder used in this work was Boehmite (Disperal sol P2, CONDEA Chemie) which changes to γ-alumina during calcination. The amount of binder used in the washcoat preparation was 20% of the total washcoat weight.

The monolith was weighted and the required amount of washcoat loading which had to be 20% of total monolith and washcoat weight was calculated. To prepare the washcoat slurry, first the calculated amount of binder was dissolved in adequate amount of milli-Q water and stirred for 30 min (stirring the solution is shown to improve the adherence effect of the binder). After that, the calculated amount of catalyst (80% of washcoat) was added to the slurry (see the appendix A for calculations).

To coat the monolith, first it was dipped in milli-Q water. This is because if the monolith is not wetted very well with the solvent, the liquid will be drawn toward monolith during drying. So the particles of the binder will lose their contact with the monolith's wall which results in very weak bonding between the catalyst particles and the monolith [54]. In the next step, the monolith was immersed in the washcoat slurry. The monolith was then taken out and the excess liquid inside the monoliths' channels was shaken out. As shown in Fig. 9, the remainder of the liquid was gently blown out by pressurized air. The monolith was then dried using a hot air gun at 90 °C in a horizontal position in order to avoid the gravity effect on washcoat distribution. Finally the monolith was calcinated at 600 °C to fix the coated layer.
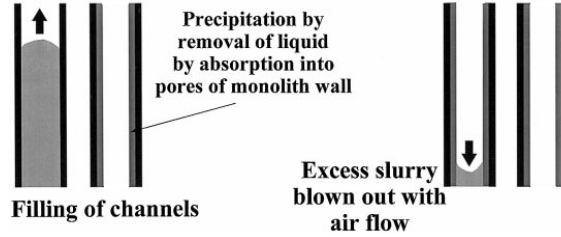
3.1.3 Catalyst characterization - specific surface area and pore size distribution

In order to determine the specific surface area and pore size distribution (PSD) of samples a Micromeritics Tristar (MT) 3000 instrument was used. First 280 mg of the F2 sample and 396 mg of the F6 sample were weighted and were put in sample tubes. Next, the sample tubes were put in an oven and heated at 200°C and under vacuum for 2 hours to remove adsorbed contaminants (especially water) obtained from atmospheric exposure. After that the sample tubes were put inside the MT; First, the samples are cooled down to 77 K by liquid nitrogen under vacuum and then they are admitted to nitrogen gas at a series of precisely controlled pressures. After each incremental dose of nitrogen gas, the pressure is allowed to equilibrate and the number of adsorbed gas molecules on the sample surface, which is defined as the adsorption isotherm, is measured and the ratio of equilibrated pressure to the saturation pressure (P/P0) along with the amount of adsorbed gas at each equilibrium pressure is recorded. The recorded values and the BET (Brunauer, Emmett and Teller) equation [58] are applied to calculate the volume of the adsorbed gas in a monolayer which is then used in calculation of specific surface area [59]:

$$S\ (m^2) = V_m (m^3) \cdot \frac{N_A}{V_A} \left(\frac{molecules}{m^3} \right) \cdot A\ (m^2)$$

Where S is specific surface area, V_m is volume of adsorbed gas in a monolayer, N_A/V_A is Avogadro's number per unit volume of gas and A is the molecular area of nitrogen (16.2 Å^2).

As adsorption continues, the adsorbed film becomes thicker and the smaller pores start to fill. The pressure is increased until the saturation is reached (P/P0 = 1) and that is when all pores on the surface are filled with nitrogen. Decreasing the pressure, the adsorbed nitrogen molecules start to leave the sample in reverse way as they were adsorbed, i.e. larger pores are emptied first. However, the gas leaves the pores at lower equilibrium pressures compared to when it entered, since it has to overcome the capillary forces inside the pores. As with the adsorption process, the amount of desorbed nitrogen gas on the solid surface at each step of decreasing equilibrium pressure is quantified. Using these two sets of data -which illustrate the adsorption and desorption isotherms- the PSD of the samples can be found by analysis of the shape of the

Table 2: Specific surface area and pore size distribution of samples.

Sample	Nominal Ag content [wt%]	Specific surface area [m^2/g]	Total pore volume [cm^3/g]	BJH absorption cumulative pore volume [cm^3/g]	Absorption average pore width [Å]	BJH absorption average pore diameter [Å]	BJH desorption average pore diameter [Å]
F2	2	193	0.25	0.24	52	46	40
F6	6	184	0.22	0.21	47	42	37

isotherms and the BJH equation [12, 60, 61]. The results from the MT instrument are shown in Table 2.

3.2 Flow-reactor experiments

The activity of the catalysts for NOx reduction and also the formation of products during experimental conditions were studied in a flow reactor. The reactor consisted of a horizontal quartz tube enclosed in a heating coil which was used as the heat supply. The coated monolith was placed inside the reactor between two uncoated monoliths in order to provide uniform temperature distribution inside the monolith by avoiding heat loss from the ends. The monolith was also sealed by quartz wool to prevent any shortcut passage for inlet gases from the sides of the monolith. A schematic overview of the flow reactor system is shown in Fig. 10.

To control the temperature inside the reactor, a thermocouple was placed before the monolith. Another thermocouple was placed inside a channel at the center of the monolith to measure the catalyst temperature. After introducing the sample monolith into the reactor, the coil and
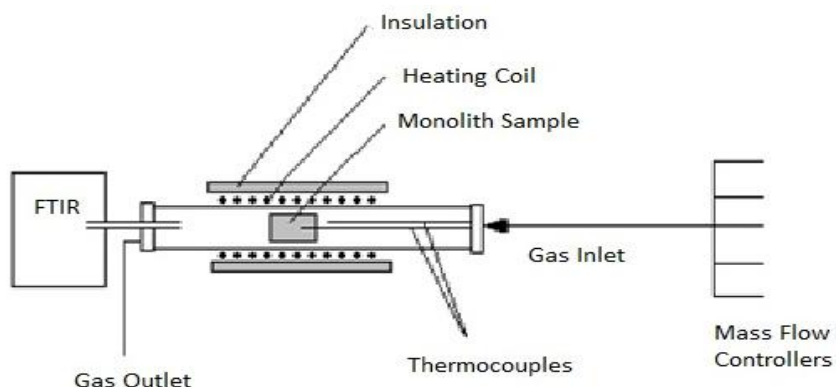
Fig. 10. Schematic view of the flow reactor set-up.

the reactor were wrapped with a thick layer of quartz wool to provide consistent heat inside the reactor. In order to control the flow rate of the reactant gases mass flow controllers (Bronkhorst Hi-Tech) were used. The exhaust gas composition from the reactor was analyzed with a MKS MultiGas 2030 HS FTIR.

The total gas flow and space velocity in all the experiments were 3500 ml/min and 32 000 h^{-1}, respectively, using argon as the carrier gas. Fig. 11 shows the step-response experiments with temperature ramps in flow reactor. At the beginning of each experiment, argon was introduced to the reactor at 20°C for a short time to set the MKS software. Following, the catalyst was pretreated in a flow of 10% O_2 for 30 minutes while the temperature was set to increase from 20°C to 550°C. In the next step, 600 ppm hydrocarbon was added to the previous gas mixture (i.e. 10% O_2, 0.6% hydrocarbon and Ar bal.) and temperature ramps (550 $\rightarrow$ 50 $\rightarrow$ 550°C, 5°C/min) were performed. Then 200 ppm NO was added to the previous gas mixture (10% O_2, 0.2% NO, 0.6% hydrocarbon and Ar bal.) and the ramps were repeated once more. Finally, the reactor was flushed with argon flow while the temperature was set to decrease to 20°C. The explained process was performed 6 times for different combinations of the catalysts (F2, F6) and the hydrocarbons (C_2H_6, C_2H_4, C_2H_2).
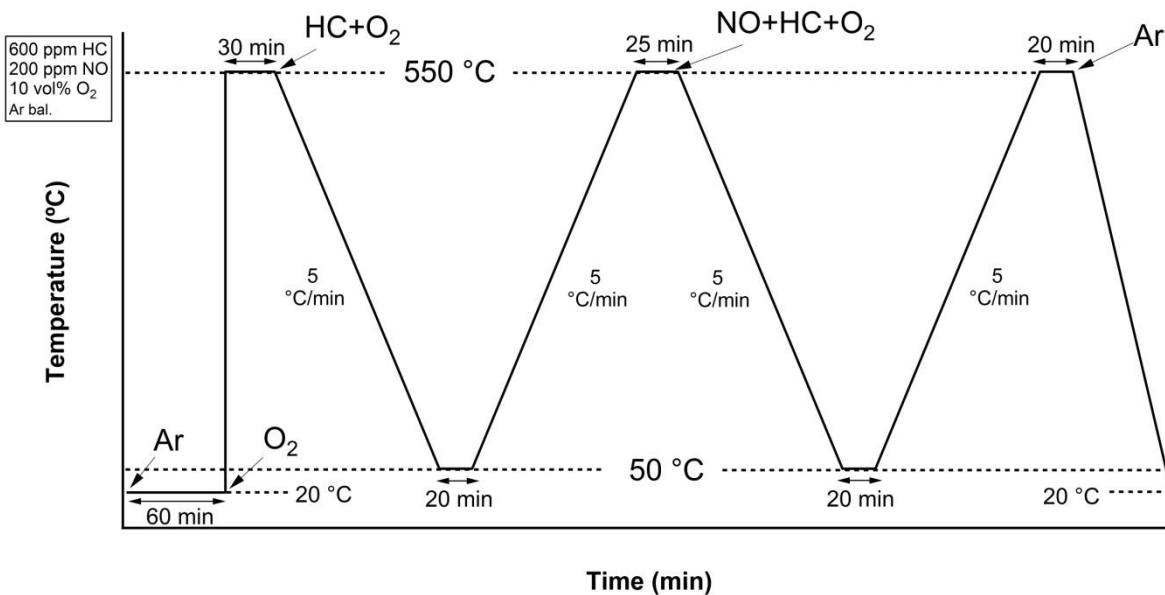
Fig. 11. Step-response experiments and temperature ramps in flow reactor.

3.3 In situ infrared Fourier transform spectroscopy experiments

The vibrational spectrum (collection of the energies associated to the vibrational transitions) of polyatomic species can be mostly obtained by direct measurements of the quality of the absorbed or emitted radiations upon these transitions. This is called IR spectroscopy which can be performed with different experimental setups [62].

Infrared spectroscopy is a known spectroscopic technique that has become popular in catalysis mainly because of its in situ (under reaction conditions) application. The most common application of this technique in catalysis is to study the adsorbed species on catalyst surface and also to distinguish how these species are adsorbed. Infrared spectroscopy can also be used to identify the present phases in precursor stages of the catalyst during its preparation. Moreover, the infrared spectra of adsorbed molecules like NO or CO can be useful for obtaining information about the absorbtion sites of a catalyst.

3.3.1 Molecular vibrations

Infrared spectroscopy is based on the ability of molecules to absorb IR radiation, i.e. photons. As molecules have discrete rotational and vibrational energy levels, the absorption of photons with a frequency (ν) in the mid-infrared range (200-4000 cm-1) enables transitions between these vibrational levels. There are four types of vibrations characteristic for different bond movements, i.e.:

- Stretch vibrations (ϑ)
- Bending vibrations in one plane (δ)
- Bending vibrations out of plane (γ)
- Torsion vibrations (τ)

A molecule can absorb infrared photons if the associated dipole moment changes during the vibration. A permanent dipole moment is thus not necessary for the molecule to be considered IR active. The intensity of the infrared band is proportional to the change in dipole moment. This is the reason for the strong IR absorption bands observed for NO and CO while species having covalent bonds, like C-C or N=N, exhibit weak absorption bands. Some molecules like H_2 and N_2 are not IR active at all [63].

3.3.2 DRIFTS

Infrared spectroscopy can be utilized in several different modes. In catalysis research, the dominating modes are the transmission/absorption and the diffuse reflection techniques. The transmition/absorbtion technique is probably the most widely used technique in infrared spectroscopy. In this technique the sample is pressed into a 1-2 centimeter self-supporting disk with thickness of a few tenths of a millimeter. Transmission infrared spectroscopy is suitable for quantitative measurements and can thus give information about the type and amount of
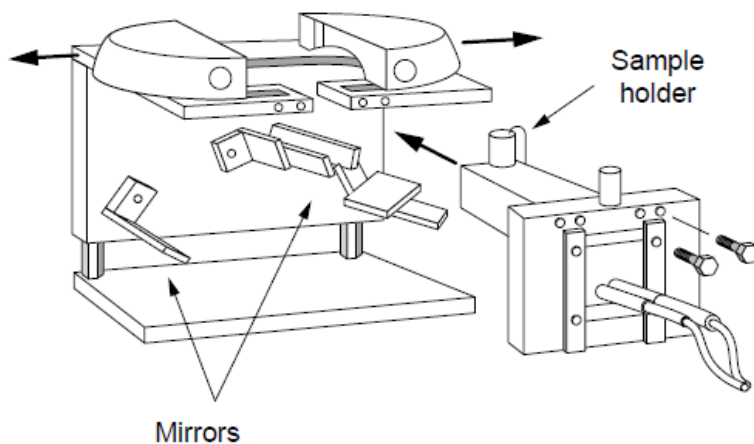
Fig. 12. Apparatus for diffuse reflection measurements [64].

adsorbed species on a surface [62, 63]. However, some samples cannot be analyzed with this technique due to the lack of mechanical strength and/or transmission. Hydrated samples or certain catalysts used for automotive pollution prevention are examples of these kinds of samples. The use of a diffuse reflection accessory and the associated DRIFTS technique helps to overcome these problems and also helps to analyze materials under reactive atmosphere without internal mass transport limitations. Furthermore, DRIFTS can be used to analyze irregular surfaces and coatings (polymer, etc.) and it is also capable of recording the spectrum of the sample at elevated temperature and pressure. However, the measurements are qualitative in DRIFTS technique and also the interpretation of the spectra obtained by this method can become difficult because they depend closely on the conditions in which they are obtained. Since the diffusion coefficient changes with each preparation, it is difficult to make a comparison between two spectra of the same material recorded in two different experiments [64]. Another problem with this technique (and also with transmission spectroscopy) is limitation of measurements for supported catalysts to frequencies above those where the support absorbs (below about 1250 cm^{-1}) [63].

Fig. 12 shows a typical DRIFTS apparatus. The infrared beam is focused by a series of mirrors on the surface of the sample that is placed inside a sample holder. Radiation diffused through the powder is collected by other mirrors and sent to the detector. Fig. 13 shows the in situ high temperature and high pressure cell. To send the gases into the dome and through the sample an inlet and outlet are provided which are shown in Fig. 14. The gases get in from the top of the sample and pass downward through the sample. The advantage of this flow direction is that the gases can be controlled thermostatically and it also makes it possible to track the surface reactions at the desired temperatures [64].
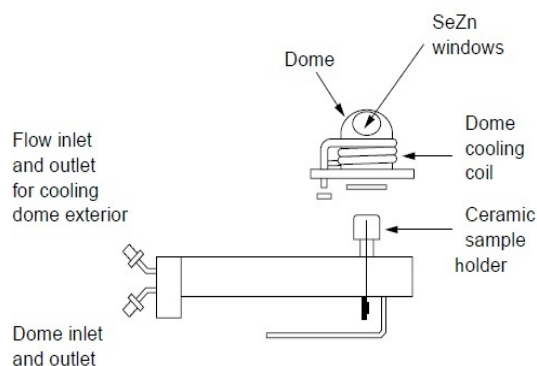
Fig. 13. Sample holder and dome [64].
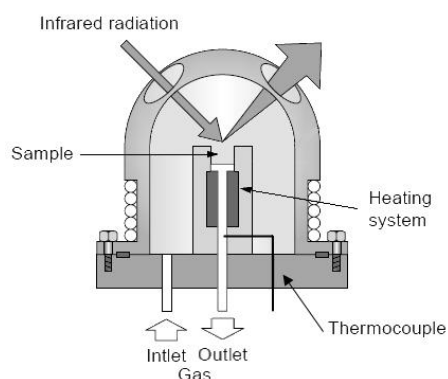
Fig. 14. Dome interior [64].

In-situ DRIFTS experiments were carried out in a BIO-RAD FTS 6000 spectrometer equipped with a high temperature reaction cell. A K-type thermocouple was used to control the temperature inside the cell. To introduce the gases to the reaction cell, mass flow controllers (Bronkhorst Hi-Tech) were used. The total flow rate in all of the DRIFTS experiments was 100 ml/min.

After placing the catalyst inside the reaction cell, it was initially pretreated in a flow of 10% O_2 (in Ar) at 500°C for 30 min and then flushed with Ar for 20 min at 450°C. Background spectra with resolution of 60 scans at 1 cm^{-1} were collected. The sample was then oxidized in a flow of 10% O_2 for 30 min at 450°C. Step-response experiments were subsequently performed at 450°C with different gas compositions of hydrocarbon, NO and O_2, shown in Table 3. During the reaction conditions the spectra were recorded in the kinetic mode, obtaining 6 scans/min at a resolution of 1 cm^{-1}. The described procedure was performed for different combinations of catalysts (F2 and F6) and hydrocarbons (C_2H_4 and C_2H_2).

Table 3: Inlet gas compositions in different steps of step-response experiments of DRIFTS.

Step	Hydrocarbon concentration (ppm)	NO concentration (ppm)	O_2 concentration (vol %)
1	600	0	10
2	0	0	10
3	600	0	10
4	600	600	10
5	0	600	10

4. Results and discussion

4.1 Catalytic activity

The results from flow reactor experiments are summarized in Fig. 15 and Fig. 16. Fig. 15 shows formation of CO and CO_2 when C_2 hydrocarbons are oxidized with O_2 over 2% and 6% Ag/Al_2O_3 (F2, F6) catalysts during temperature ramp down (extinction). For the F2 catalyst, acetylene (C_2H_2) has the lowest activation temperature (around 250°C) compared to the other hydrocarbons and this hydrocarbon shows significantly higher CO and CO_2 production (two times more in CO_2 case). CO formation with acetylene has maxima around 450°C, and above this temperature CO_2 formation is favored. The activation temperature for both ethene (C_2H_4) and ethane (C_2H_6) is around 450°C and the CO_X formation is nearly the same in both cases. The results in Fig. 15 indicates that ethene and ethane do not reach their light-off temperature (in this work defined as the temperature corresponding to 50% conversion of the hydrocarbon [65, 66]) for any of the two catalysts.

Comparing the F6 and F2 catalysts, some differences are noticeable. The activation temperatures for C_2H_2 and C_2H_4 are lower in the F6 catalyst (approximately 350°C and 450°C, respectively), compared to the F2 catalyst, however for C_2H_6 the activation temperature is similar over both catalysts. Oxidation of C_2H_2 over the F2 catalyst results in a higher formation of CO compared to the F6 catalyst. On the other hand, formation of CO and CO_2, when C_2H_4 and C_2H_6 are oxidized, is higher in the F6 catalyst.
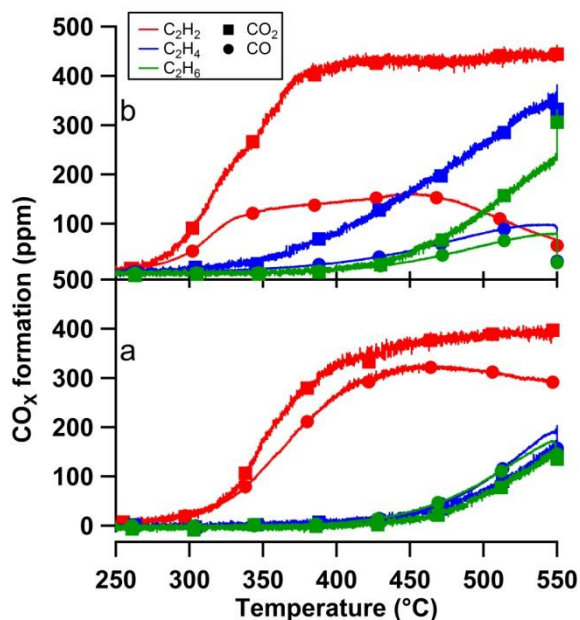
Fig. 15. Formation of CO (Circle marks) and CO_2 (square marks) due to combustion of C_2 hydrocarbons over Ag/Al_2O_3 catalyst with (a) 2 wt% (F2) and (b) 6 wt% (F6) nominal silver content. Inlet gas flow composition: 600 ppm C_2 hydrocarbon, 10% O_2,Ar balanced. GHSV: 32 000 h^{-1}.

24
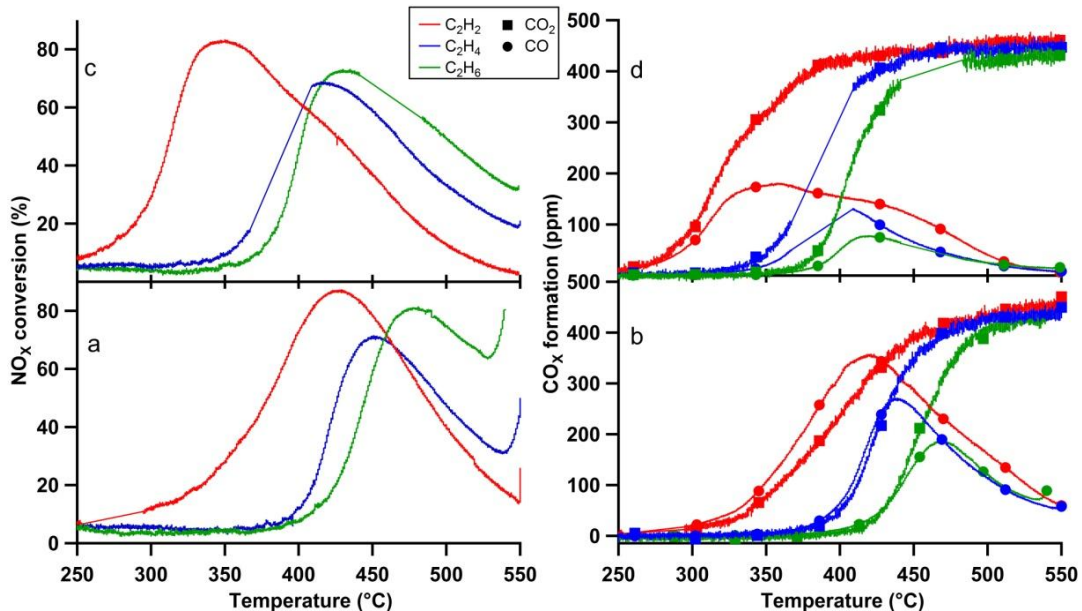
Fig. 16. Formation of CO (Circle marks) and CO₂ (square marks) due to combustion of C_2 hydrocarbons (right side) and NO_X conversion (left side) over Ag/Al_2O_3 catalyst with (a, b) 2 wt% (F2) and (c, d) 6 wt% (F6) nominal silver content. Inlet gas flow composition: 200 ppm NO, 600 ppm C_2 hydrocarbon, 10% O_2, Ar balanced. GHSV: 32 000 h^{-1}.

In the oxidation reaction of acetylene over both F2 and F6 catalysts, small traces of formaldehyde (2 ppm) was detected at 350°C and 300°C, respectively (see appendix A). Moreover, very small amount of methane (1-2 ppm) was traced in both cases for all of the hydrocarbons. The strange behavior of some of the curves in Fig. 16 at 550°C (e.g. increase in NO_X conversion) is due to SGB software problem in reading a part of the defined sequence file. In that part adding of NO was supposed to take place 300 seconds before starting the ramps but it was started at the beginning of the ramp down.

Fig. 16 shows the NO_X reduction and CO_X formation for the reduction of NO by C_2 hydrocarbons in the presence of excess O_2 over the F2 and F6 catalysts during temperature ramp down (extinction). Comparing different reductants for the F2 sample, acetylene shows the highest NO_X conversion (87% at 427°C) and also the widest temperature window (temperature interval where NO_X conversion is detected) for NO_X reduction. The maximum NO_X reduction for ethylene and ethane are 71% at 451°C and 81% at 481°C, respectively. The temperature windows for these hydrocarbons are similar, showing no significant activity below 400°C. At temperatures above 460°C, ethane shows higher NO_X reduction compared to the two other hydrocarbons. NO_X reduction over the F6 catalyst follows the same pattern, however, the maximum NO_X reduction is slightly decreased for all the reductants and its corresponding temperature is shifted to lower temperatures.

25

Comparing CO_X formation over F2 catalyst in this step (Fig. 16.c) with the previous step (Fig. 15.a), acetylene still has the lowest activation temperature and the maximum level of CO_2 production is raised to 450 ppm (from 400ppm). CO_X formation when using ethylene and ethane is drastically different if NO is present in the feed gas. In particular the formation of CO is significantly increased and the activation temperatures are shifted to lower temperatures compared to the oxidation experiments (without NO). The CO_X formation over F6 catalyst follows the same trends as the F2 catalyst but with lower activation temperatures and lower CO formation. These changes may be explained by the fact that NO_X is a stronger oxidizing agent than O_2, especially in the form of nitrates and can likely promote the activity of hydrocarbons [67]. When NO was present in the feed, small concentrations (lower than 5 ppm) of NH_3, N_2O and HCHO were detected among the gas phase products but no trace of HCNO and HCOOH were found. The strange behavior in the C_2H_4 curves (370-415°C) is due to unrecorded data by FTIR software (MKS). The missing data are substituted with a straight line.

An interesting feature is that the temperature corresponding to the maximum CO formation coincides with the temperature for maximum NO_x reduction, for both catalysts. This is likely related to partial oxidation of the hydrocarbons, since CO is a product of partial oxidation. It is known that partially oxidized hydrocarbons are key intermediates in the SCR process, so the temperature corresponding to the maximum formation of partially oxidized hydrocarbons is likely close to the temperature for maximum NO_X reduction. Another possibility is that CO itself may act as an intermediate in the lean NO_x reduction.

The results from the flow reactor experiments show that increasing the silver loading (from 2 to 6 wt%), shifts both the NO_X removal temperature range and the activation temperature of the hydrocarbon to lower temperature regions and also broadens the NO_X reduction temperature window. These changes are probably caused by the presence of higher amounts of metallic silver species in the F6 catalyst compared to the F2 catalyst. These findings are in agreement with the results in previous studies [52, 68]. This may explain the lower CO and higher CO_2 concentrations observed for the F6 catalyst, compared to the F2 catalyst, which likely is caused by favoring total oxidation of hydrocarbons forming CO_2 rather than CO over the F6 catalyst. Low temperature activation of hydrocarbons accompanied by high NO_X reduction ability over the catalyst samples indicate high distribution of both oxidizing (metallic silver, $Ag_n^{\delta+}$ clusters) and reducing (such as Ag^+, Ag_2O) silver species through the catalytic material.

From the flow reactor results, the activation of C_2 hydrocarbons over F2 and F6 catalysts can be arrayed in the order: $C_2H_2 > C_2H_4 > C_2H_6$. However, the ability of these hydrocarbons for NO_X reduction in lean conditions follows a different order: $C_2H_2 > C_2H_6 > C_2H_4$. It may seem odd that the activation of acetylene is easier than activation of ethene and ethane, even though the former has the strongest C-C bond. However, the comparison between the hydrocarbons should

be based on bond energies per electron pair. This energy for acetylene is 835(C≡C)/3 = 278 KJ/mol and for ethene is 615 (C=C)/2 = 308 KJ/mol while this energy for ethane (single C-C bond) is 345 KJ/mol. Therefore, the triple bond of acetylene is stronger however more reactive than the double bond of ethene or the single bond of ethane. The double bond of ethene, in turn, is stronger but more reactive than the single bond of ethane [69].

Another matter that can influence the activity of the C_2 hydrocarbons is the efficiency of sideway orientation interaction between C-H bond of the hydrocarbon and the metal. Clearly, acetylene can reach this position more easily than ethene and ethane. The easiness of this interaction for ethene can be placed between acetylene and ethane. Ethane, on the other hand, needs the largest initial disorientation of the molecule to reach a proper interaction [70].

4.2 Surface species and mechanisms

4.2.1 Surface species

The DRIFTS peaks/bands attributed to evolution of surface species during various reaction conditions, and their assignments, are summarized in Table 4. Fig. 17 shows the DRIFTS spectra of surface species formed in the step-response experiments over the F2 and F6 catalysts at 450°C, with ethene as reductant. When ethene and oxygen are introduced to the F6 catalyst (step 1), bands at 1248, 1296, 1459, 1545, 1570, 1588, 2906 and 2997 cm^{-1} appear. The bands at 1245, 1296 and 1545 cm^{-1} are assigned to $\vartheta_{as}(COO)$ of bidentate and monodentate carbonates, respectively. The bands at 1459 and 1570 cm^{-1} are assigned to $\vartheta_{as}(COO)$ of acetate or free carboxylate species. The peak at 1588 cm^{-1} and the weak bands at 2906 and 2997 cm^{-1} are respectively ascribed to $\vartheta_{s}(COO)$, $\vartheta (CH)$ and $\vartheta_{s}(COO)+ \vartheta (CH)$ of formate. For the F2 catalyst, bands at 1250, 1294, 1378, 1391, 1457, 1545, 1588 cm^{-1} and weak peaks at 2906 and 2997 cm^{-1} (not shown) were observed. A majority of these bands are similar to the ones observed for the F6 catalyst and can be assigned accordingly. The bands at 1378 and 1391 cm^{-1}, however, are only observed for the F2 sample and may be assigned to $\vartheta_{s}(COO)$ of formate.

In step 2, when ethene was switched off, the acetate bands at 1459 and 1570 cm^{-1} are gradually decreasing for both catalysts. In step 3, after ethene was switched on again, the acetate bands grow back to their previous positions (as in step 1). After adding NO, in step 4, new bands at 1245, 1292, 1378, 1391, 2245 cm^{-1} appear, while the acetate band at 1459 cm^{-1} disappears for both the F2 and F6 catalyst (because of the overlaps, the changes in another band of acetate at 1570 cm^{-1} was not distinguishable). The peaks at 1245 and 1292 cm^{-1} are attributed to $\vartheta_{as}(NOO)$ of monodentate or bidentate nitrates. The weak band at 2245 cm^{-1} can be attributed to –NCO or NO^{+} species. For the F2 sample bands evolve at 1250, 1294 and 2245 cm^{-1}, these are similar to the bands observed for the F6 sample and are assigned accordingly. The intensity of
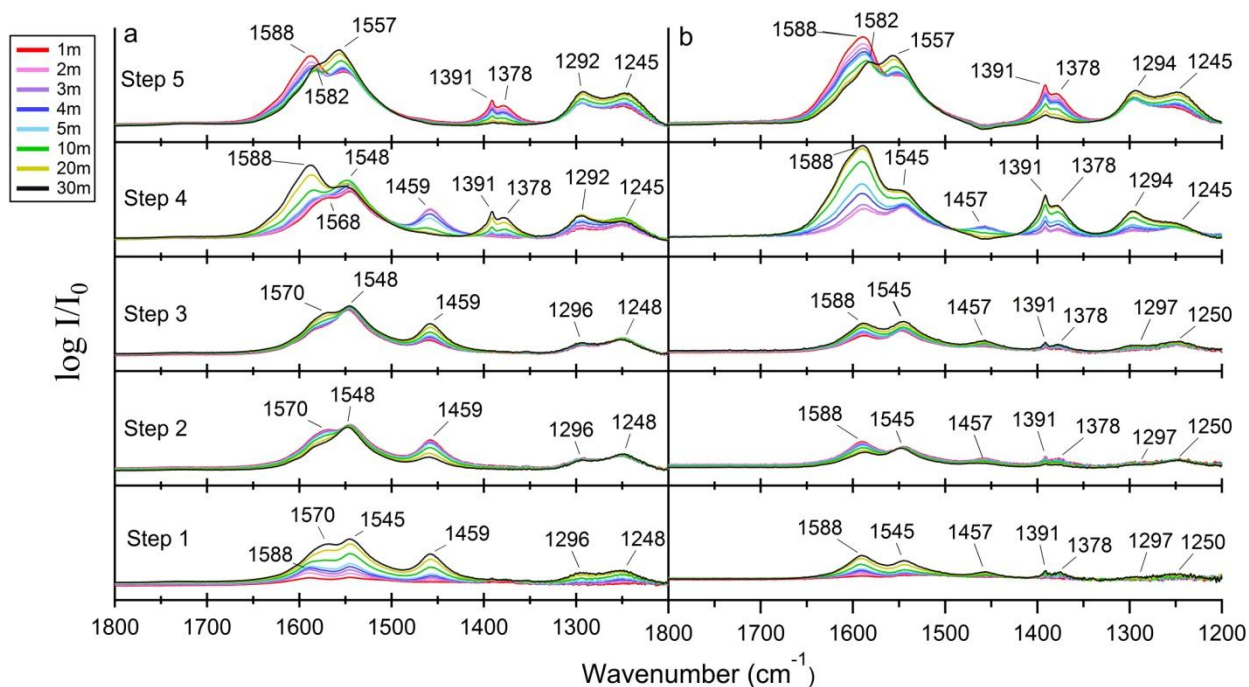
Fig. 17. Step response experiments for ethene recorded in DRIFTS at 450°C over Ag/Al_2O_3 catalyst with (a) 6 wt% (F6) and (b) 2 wt% (F2) nominal silver content. Red to black lines (legend): 1 to 30 min after gas exposure. Inlet gas flow composition for step 1: $C_2H_4+O_2$; step 2: O_2; step 3: $C_2H_4+O_2$; step 4: $C_2H_4+NO+O_2$; step 5: $NO+O_2$. Contents: 600 ppm NO, 600 ppm C_2H_4, 10% O_2, Ar balanced.

the formate bands at 1588, 2906 and 2997 cm^{-1} seems to increase for both catalysts during this step, while the intensity of the carbonate bands rather are reduced (however it is not very clear because of the overlapping with nitrate bands).

Switching off ethane, in step 5, new bands at 1557 and 1582 $cm^{-1}$are observed ($\vartheta_{as}(NOO)$, $\vartheta_{as}(NOO)$ of monodentate and bidentate nitrate, respectively) for both catalysts. The formate bands gradually decrease and the intensity of the bands at 1245/1250 and 1292/1294 cm^{-1} (nitrates) simultaneously increase.

Fig. 18 shows the evolution of DRIFTS spectra obtained in similar reaction conditions as Fig.17 but using acetylene as reductant (instead of ethane). After introducing acetylene and oxygen in the first step, several bands are detected for the F2 and F6 catalysts. For the F2 catalyst (Fig. 18.b), several bands at 1298, 1354, 1391, 1460, 1539, 1576 cm^{-1} and very weak peaks at 2903, 2942, 2997 and 3017 cm^{-1} (not shown) appear. Most of these bands are similar to the bands observed in the previous experiments (see Table 3 for the assignments of these bands). New bands at 1354, 2942 and 3017 cm^{-1} can be ascribed to $\vartheta(CH_3)$ of acetate, $\vartheta_{as}(CH)$ of methylene and ϑ (CH) of C=CH2. For the F6 catalyst, bands at 1298, 1340, 1412, 1460, 1542, 1576, 1627, 2942 and 3027 cm^{-1} are observed. Some of these bands are assigned previously (see Table 4), however, 1340, 1412 and 1627 cm^{-1} are new and can be assigned to both enolic ($\delta(CH)$, $\vartheta_s(RCH=CO)$ and $\vartheta_{as}(RCH=CO)$, respectively) and carbonate ($\vartheta_{as}(COO)$) species. The peak
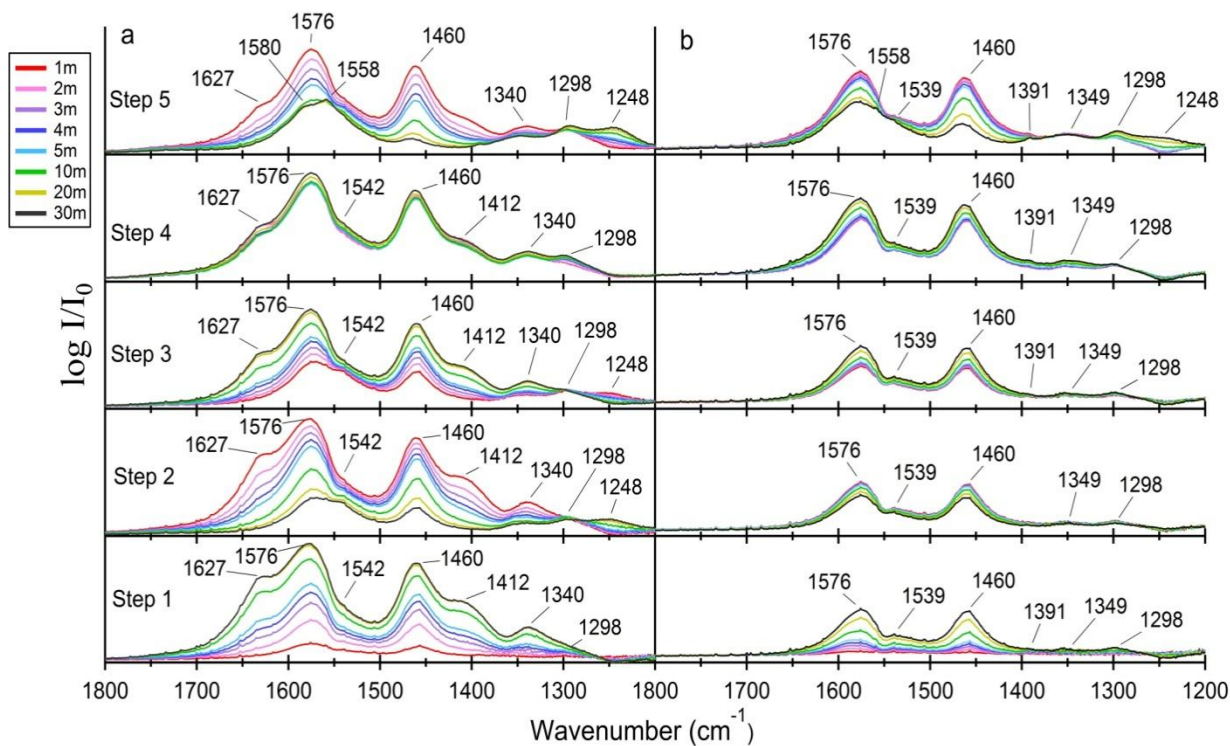
Fig. 18. Step response experiments for acetylene in a DRIFTS at 450°C over Ag/Al₂O₃ catalyst with (a) 6 wt% (F6) and (b) 2 wt% (F2) nominal silver content. Red to black lines (legend): 1 to 30 min after gas exposure. Inlet gas flow composition for step 1: $C_2H_2+O_2$; step 2: O_2; step 3: $C_2H_2+O_2$; step 4: $C_2H_2+NO+O_2$; step 5: $NO+O_2$. Contents: 600 ppm NO, 600 ppm C_2H_2, 10% O_2, Ar balanced.

at 1627 cm^{-1} is also ascribed to C=O stretch of formyl or aldehyde species.

In step 2 (switching off acetylene), the intensity of all bands are reduced except the band at 1248 cm^{-1} which can probably be due to formation of carbonate species in presence of oxygen. The bands, in this step, show more reduction in intensity over F6 catalyst compared to F2 catalyst which may be due to the presence of more metallic silver particles in F6 catalyst. Switching on the acetylene in step 3, the peaks are regenerated and the peak at 1248 cm^{-1} diminishes. However, the intensities of the regenerated bands on the F6 catalyst are lower compared to step 1. When adding NO to acetylene and oxygen (step 5) new peaks at 2124 and 2228 cm^{-1} for the F6 catalyst and at 2124, 2151 and 2228 cm^{-1} for the F2 catalyst arise, *cf.* Fig. 19, and also the intensity of previous peaks are slightly increased. The peaks at 2124 and 2151 cm^{-1} are ascribed to cyanide (-CN) species bonded to Ag or Al and the band at 2228 cm^{-1} is attributed to isocyanate (–NCO) species attached to Ag or Al atoms at the catalyst surface. The nitrate bands usually overlap with acetate and carbonate peaks and in this experiment it seems that peaks corresponding to nitrate species are covered by acetate and carbonate bands. In step 6, after removing acetylene from the feed gas, bands at 1248, 1298, 1558 and 1580 cm^{-1} appear, which are previously assigned to monodentate and bidentate nitrates. During this step the

intensity of the other bands resulting from the acetylene reaction (carboxylates and carbonates) reduces.

Table 4: Summation of observed peaks in this study and their assignments.

Surface species	Observed Bands (cm-1) C$_2$H$_4$	C$_2$H$_2$	Assignment	Reference Bands (cm-1)	Ref
CHO	1248	-----	ϑ_{as}(COO) of bidentate carbonate	1270-1250	[71]
			δ(COH) of bicarbonate	1230	[72]
	1296	1298	ϑ_{as}(COO) of monodentate carbonate	1370-1300	[71]
			ϑ_{as}(COO) of bidentate carbonate	1440-1320	[72]
	1378	-----	δ(CH) of formate	1378	[73]
			ϑ_s(COO) of formate	1380,1375	[46, 74]
	1391	1391	ϑ_s(COO) of formate	1390	[72]
			δ(CH) of formate	1390	[46, 74]
	-----	1340	δ(CH) of enolic species	1336, 1333	[75, 76]
			ϑ_{as}(COO) of (ethyl) carbonate	1340,1336	[33, 74]
	-----	1354	ϑ(CH$_3$) of Acetate	1355	[73, 77]
	-----	1412	ϑ_s of enolic species (CH$_2$=CH-O$^-$)	1416,1412	[75, 76]
			ϑ_{as}(COO) of (ethyl) carbonate	1412	[33, 74]
	1459,1457	1460	ϑ_s(COO) of acetate/ free carboxylate	1466-1460	[33, 73, 76, 78]
	1548,1545	1539,1542	ϑ_{as}(COO) of Monodentate Carbonate	1680-1530	[71]
	1570	1576	ϑ_{as}(COO) of acetate/ free carboxylate	1580-1570	[33, 73, 76, 78]
	1588	-----	ϑ_s(COO) of formate	1595,1593	[46, 74]
	-----	1627	C=O stretch of formyl or aldehyde	1635	[79]
			ϑ_{as} of enolic species (CH$_2$=CH-O$^-$)	1633,1630	[75, 76]
			ϑ_{as}(COO) of (ethyl) carbonate	1630,1626	[33, 74]
	2906	2903	ϑ (CH) of formate	2917,2910	[46, 80]
	-----	2942	ϑ_{as}(CH) of methylene	2935	[81]
	2997	-----	ϑ_s(COO)+ ϑ (CH) of formate	3005	[46]
		3027,3017	ϑ (CH) of C=CH	3020	[81]
NO$_X$	1245	1248	ϑ_{as}(NOO) of monodentate/bidentate nitrate	1245-1250	[82, 83]
				1250-1290	[84]
	1292	1298	ϑ_{as}(NOO) of monodentate/bidentate nitrate	1298,1297	[82, 83]
				1300-1260	[83]
	1557	1558	ϑ_{as}(NOO) of monodentate nitrate	1560,1550	[82, 83]
				1530-1480	[83]
	1582	1580	ϑ_{as}(NOO) of bidentate nitrate	1590,1585	[82, 83]
				1565-1500	[84]
-NCO/ -CN	-----	2124	Ag/orAl-CN	2130,2127	[44, 74]
	-----	2151	Ag/orAl-CN	2162,2155	[44, 74]
	-----	2228	Al(IV)-NCO	2228	[74]
			Ag-NCO	2235	[82]
			NCO bound to Ag$^+$ ions	2232	[44]
	2245	-----	Al(VI)-NCO	2255	[74]
			Nitrosonium (NO$^+$)	2311-2237	[85]
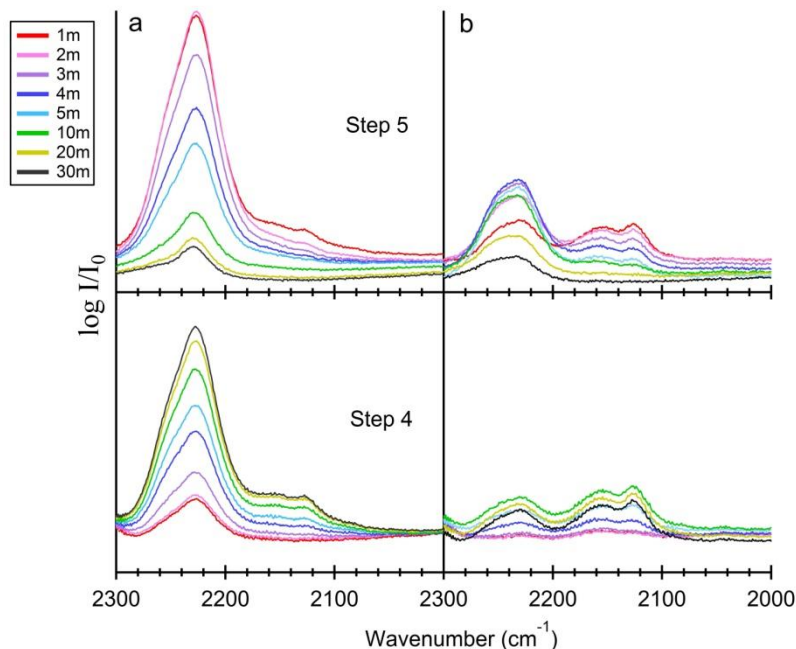
Fig. 19. Evolution of isocyanate an cyanide peaks in DRIFTS experiments with acetylene at 450°C over Ag/Al$_2$O$_3$ catalyst with (a) 6 wt% (F6) and (b) 2 wt% (F2) nominal silver content. Red to black lines (legend): 1 to 30 min after gas exposure. Inlet gas flow composition for step 4: C$_2$H$_2$+NO+O$_2$; step 5: NO+O$_2$. Contents: 600 ppm NO, 600 ppm C$_2$H$_2$, 10% O$_2$, Ar balanced.

4.2.2 Mechanistic aspects

The initial steps in the HC-SCR mechanism are formation of surface nitrates by oxidation of adsorbed NO$_x$ and formation of hydrocarbon derived surface oxygenates, such as acetate, and enolic species, by partial oxidation of hydrocarbon with oxygen. The adsorbed acetate or enolic species can then react with nitrates to form N$_2$ or organo-nitro and -nitrite species (R-ONO and R-NO$_2$) which can lead to the formation of –NCO and/or –CN species. These species can further react with nitrates and O$_2$ to form N$_2$ or can be hydrolyzed by water to form NH$_3$ which can also react with NO$_x$ to produce N$_2$ [44, 81, 86]. The reaction path, however, can vary in different studies mainly because of the difference in reactants, reaction conditions and catalyst type and preparation [44, 74, 77, 81, 82, 87].

Experiments with flow reactor are like studying a black box in which only the inlet and outlet components are known. DRIFTS experiments help to get a better understanding from inside of this black box by revealing the participating intermediates in the reactions that take place. However, as mentioned before, it is difficult to compare spectra from different experiments of DRIFTS. Therefore, the comparisons in this work are not based on the measured intensities of the bands but are rather comparisons of ratios between bands in the same experiment. Further, this should be viewed as a qualitative discussion on possible reaction intermediates and pathways.

The basic fact that can be deduced from the evolution of different peaks in DRIFTS results is that the type of reductant plays a more important role in the nature of formed surface compounds than the catalyst loading does. Using ethene as reductant, acetate, formate and carbonates are the main products of the hydrocarbon oxidation and the evolution of the peaks related to these species nearly follow the same trend for both of the catalysts. Moreover, no cyanide species are formed on the surface of the catalysts in this case. Using acetylene as reductant, the evolution of surface species in different steps shows some similarity between F2 and F6 catalysts. For instance, for both of the catalysts a similar peak at 2942 cm^{-1} is formed which cannot be observed while ethene is used as reductant. In addition, both isocyanate and cyanide species are detected for both catalysts whereas no cyanide is observed on catalysts surface with ethene as reductant.

Another fact is the formation of more surface species on the F6 catalyst compared to the F2 catalyst, for each reductant. This is probably because of the presence of more metallic silver particles in the F6 catalyst which can result in easier activation for hydrocarbons, leading toward formation of more surface species.

Using ethene as reductant, the acetate surface species diminish when NO is added to the feed gas in step 4 (for both catalysts). There may be several reasons for this behavior; one possibility can be total transformation to a different surface species (probably formate). Another possibility is higher rate of consumption of acetate in the reaction with surface nitrates than the rate of formation by partial oxidation of reductant. However, the DRIFTS spectra of ethene show negligible indications of –NCO and –CN species on the catalysts surface (both for F2 and F6), except for a faint peak around 2240 cm^{-1}. Considering the existence of the very weak band at 2240 cm^{-1} (–NCO species) and observing that this band and the band related to formate remain until 30 min from when ethene was switched off, when no acetate are left on the surface, it seems likely that formate plays a role in the formation of –NCO species. Moreover, higher NO$_X$ reduction on F2 (71%) than F6 (59%) at 450°C accompanied by higher formate-to-acetate ratio (e.g. after 10 min in step 4) for F2 catalyst can be considered as another evidence for the role of formate in the NO$_X$ reduction.

As mentioned before, there is no clear evidence (in this work) for the formation of –NCO and –CN species for ethene as reductant, except for a faint band. There are two possible reasons for this phenomenon. Firstly, the rates of formation and consumption of these species are equal; secondly, no such species are formed on the surface at all and the faint band at 2245 cm^{-1} can be due to nitrosonium (NO$^+$) species. Considering the second reason, one may assume that the main reduction mechanism for ethene does not follow the –NCO and –CN species formation path. For example, it may proceed through reduction of adsorbed nitrates by acetate to form N$_2$.

An interesting feature in the DRIFTS experiments is the formation of formate. Arranging the experiments in step 4 based on the formate-to-acetate ratio after 10 min, the following order is obtained: F2-C_2H_4 > F6-C_2H_4 > F2-C_2H_2 > F6-C_2H_2. As discussed before in flow reactor results, F6 catalyst is more active than F2 catalyst for oxidation reactions and C_2H_2 is a more active hydrocarbon compared to C_2H_4 and can be oxidized at lower temperatures. Therefore, the shown order is arranged from lowest to highest hydrocarbon oxidation performance. This indicates that the probability of formate formation is decreased by higher oxidation possibility. In other words, the tendency towards formation of formate species increases in less active environment (less active reductant and less active catalyst for oxidation).

In a SCR study by n-octane as reducing agent over Ag-Al_2O_3, Shimizu *et al*. [33] have observed the bands at 1340, 1412 and 1627 cm^{-1} and have assigned them to carbonate species and claim that these species can cause a poisoning effect. These findings are in agreement with our study which shows lower NO_X conversion for F6 (where bands are observed) than F2 catalyst when acetylene is used as reductant. The poisoning effect of these species can be the reason for hindering the NO_X conversion over F6 catalyst.

He *et al.* [81] have attributed the peaks at 1340, 1412 and 1627 cm^{-1} to enolic species, using C_2H_5OH as reductant in their study. They claim that on the Ag/Al_2O_3 surface, the acetate is predominant within a high temperature range (500–600 °C), while enolic species become dominant at a low temperature range (200–400 °C). Furthermore, they suggest that enolic surface species are more reactive toward formation of –NCO and –CN species on the catalyst surface. Based on these findings, it is expected that at a certain temperature the ratio of acetate to enolic species be higher for F6 catalyst compared to F2 catalyst because of its higher activity. However, in our study, the enolic species are only observed on F6 catalyst which can be interpreted as lower acetate to enolic species and the NO_X conversion is lower for F6 catalyst at 450 °C. One explanation for these results can be that enolic species cannot form on F2 catalyst even at lower temperatures. Another explanation can be that the temperature at F6-C_2H_2 experiment was lower than the temperature at F2-C_2H_2 experiment due to probable problems with the instruments. Examining the variations of the –NCO and –CN species in steps 4 and 5 for F6 catalyst, as far as no changes where noticed for C-containing species in step 4, it is not possible to state clearly what species (acetate and/or enolic) are participating in the formation of –NCO and –CN species. In step 5, after 30 min, no traces of any enolic species can be observed, while both acetate and –NCO bands indicate that these species still remain on the catalyst's surface. The intensity of the –NCO band may imply the formation of new –NCO species likely via acetate reaction or can be an indication of accumulated –NCO species on the surface.

5. Conclusions

A series of experiments for the silver-alumina HC-SCR catalyst were carried out using flow reactor and DRIFTS. The effect of type of hydrocarbons (C_2H_2, C_2H_4 and C_2H_6) and silver loading (2% and 6%) on the catalytic properties were studied. The flow reactor experiments show that the highest activity for NO_x reduction is achieved when C_2H_2 is used as reductant. This is in accordance with the lower binding energy per bond and easier interaction with metal for C_2H_2 compared to the other C_2 hydrocarbons. The NO_x reduction temperature window is broadened and shifted towards lower temperatures as the number of C-C bonds increase for the C_2 hydrocarbons studied. Comparisons between the catalysts with 2% Ag (F2) and 6% Ag (F6) show higher oxidative ability for the F6 catalyst. A good agreement is found between the temperature corresponding to the highest CO formation and highest NO_x conversion for each hydrocarbon.

DRIFTS experiments reveal the presence of different surface species on the catalysts. Comparing the different types of reductant and the silver loading, the type of reductant seems to have a larger effect on the nature of formed species and on the reaction mechanism, than the silver loading. Comparing the F2 and F6 catalysts, F6 shows higher formation of surface species, probably because of the presence of more metallic silver particles in this catalyst. The following order was obtained based on the formate to acetate ratio: F2-C_2H_4 > F6-C_2H_4 > F2-C_2H_2 > F6-C_2H_2, which shows that formate surface species formation is likely favored in a less oxidative environment.

6. Future work

The differences in formation of adsorbed species on the catalyst surface and the subsequent reactions can be further investigated with *e.g.* isotope labeled reactants to be able to track the "individual" atoms during reaction. DRIFTS experiments can be carried out at different temperatures to examine the effect of temperature on the formation of surface species.

Acknowledgements

This work was performed at the Competence Centre for Catalysis and Applied Surface Chemistry, Chalmers University of Technology.

Here, I would like to give my special thanks to:

Hanna Härelind Ingelsten and Per-Anders Carlsson, my supervisors, for all their supports, time and constructive discussions and comments from the initial conception to the end of this work and always being available for questions whenever I needed it.

My examiner, Professor Magnus Skuglundh, for his great comments on this work.

Fredrik Gunnarsson, for all his helps with everything and also for the great talks.

All the friends at KCK and Applied Surface Chemistry for making an enjoyable time for me during my work.

My parents, for for their dedication and the many years of support during my studies.

Fatemeh, my wonerful wife, for her love and her constant support and encouragement. You opened my eyes to a new life!

Appendix

A. Calculations regarding catalyst preparation

MW:

AgNO3 = 16.87   g/mol

Ag = 107.87   g/mol

AIP (Aluminum Isopropoxide – C9H21AlO3) = 204.24   g/mol

Al = 26.98   g/mol

Al2O3 = 101.96   g/mol

2% sample:

We want to prepare 5 g Ag/Al2O3 sample with 2% Ag so the amount of Ag in the sample should be 5*0.02 = 0.1 g

The precursor used for Ag is AgNO3. To find the amount of silver nitrate needed:

$$0.1 \ g \ Ag * \frac{1}{107.87} \ \frac{mol \ Ag}{g \ Ag} * \frac{1 \ mol \ AgNO3}{1 \ mol \ Ag} * 169.87 \ \frac{g \ AgNO3}{mol \ AgNO3} = 0.157$$

As AgNO3 was supposed to be dissolved in MQ at 1:10 weight ratio nearly 1.575 g of MQ water is needed. The rest of the sample should contain alumina so the amount of alumina needed is 4.9 g. the precursor used for alumina was AIP. The amount of AIP needed to get 4.9 g of alumina is:

$$4.9 \ g \ Al2O3 * \frac{1 \ mol \ Al2O3}{101.96 \ g \ Al2O3} * \frac{2 \ mol \ Al}{1 \ mol \ Al2O3} * \frac{1 \ mol \ AIP}{1 \ mol \ Al} * 204.24 \ \frac{g \ AIP}{mol \ AIP} = 19.631$$

B. Flow reactor plots

HC+O₂:
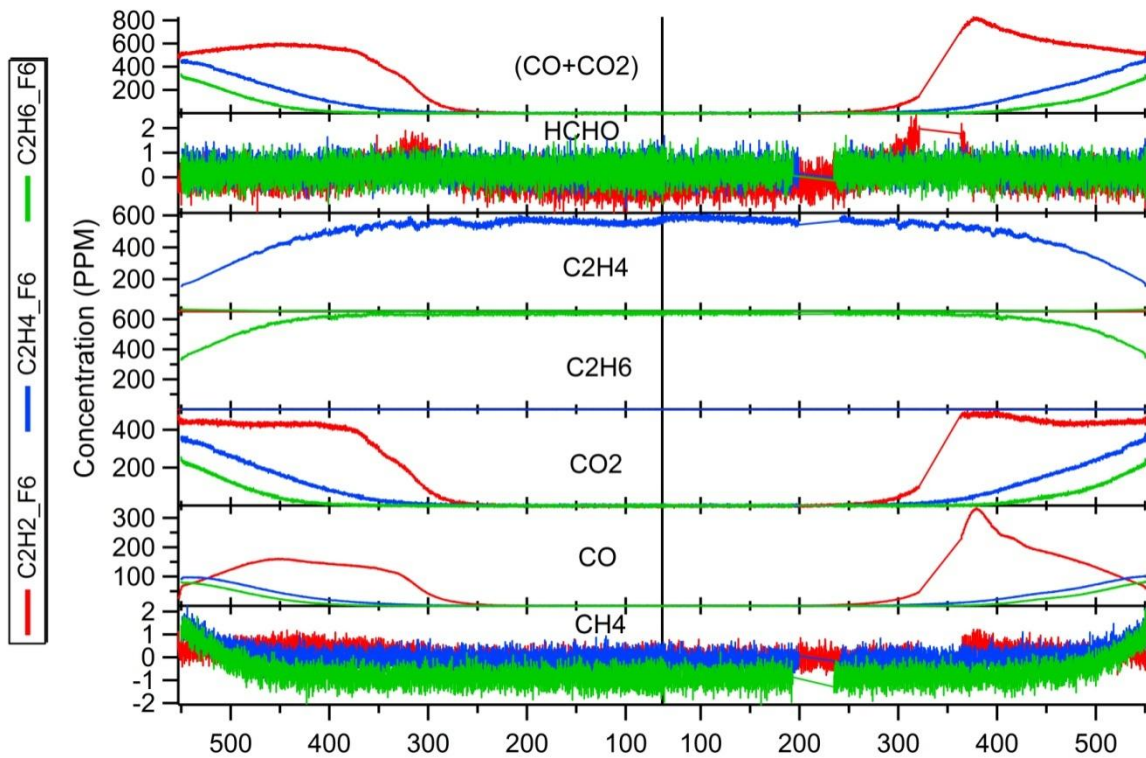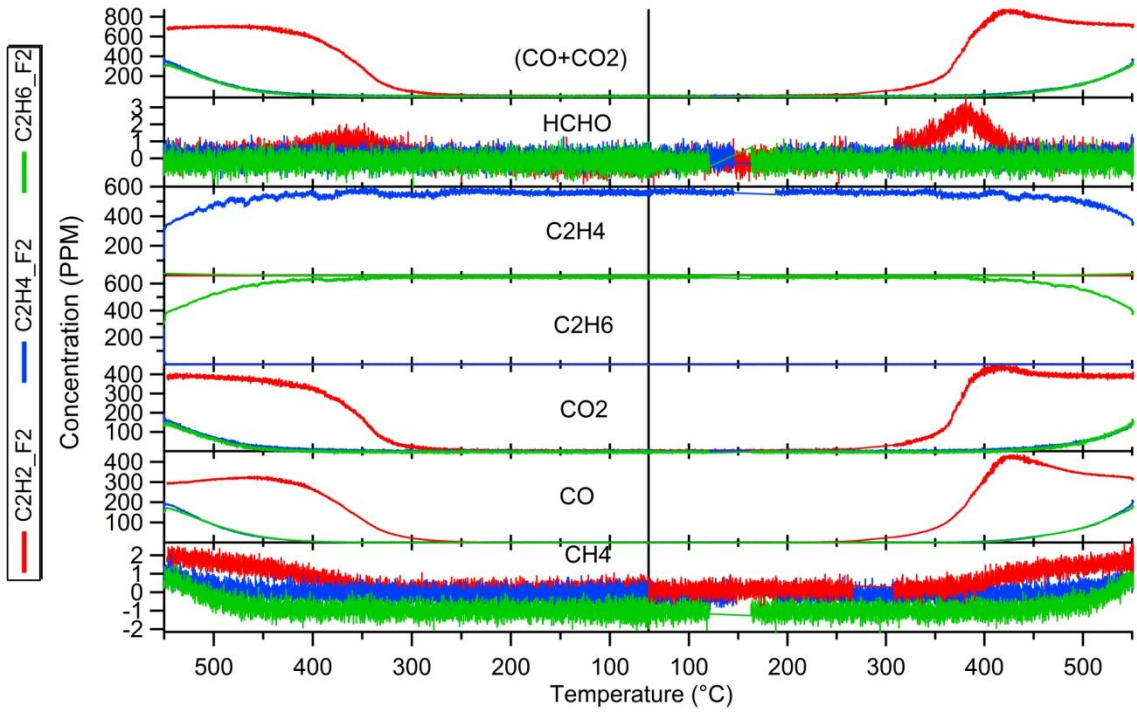
HC+O₂+NO:
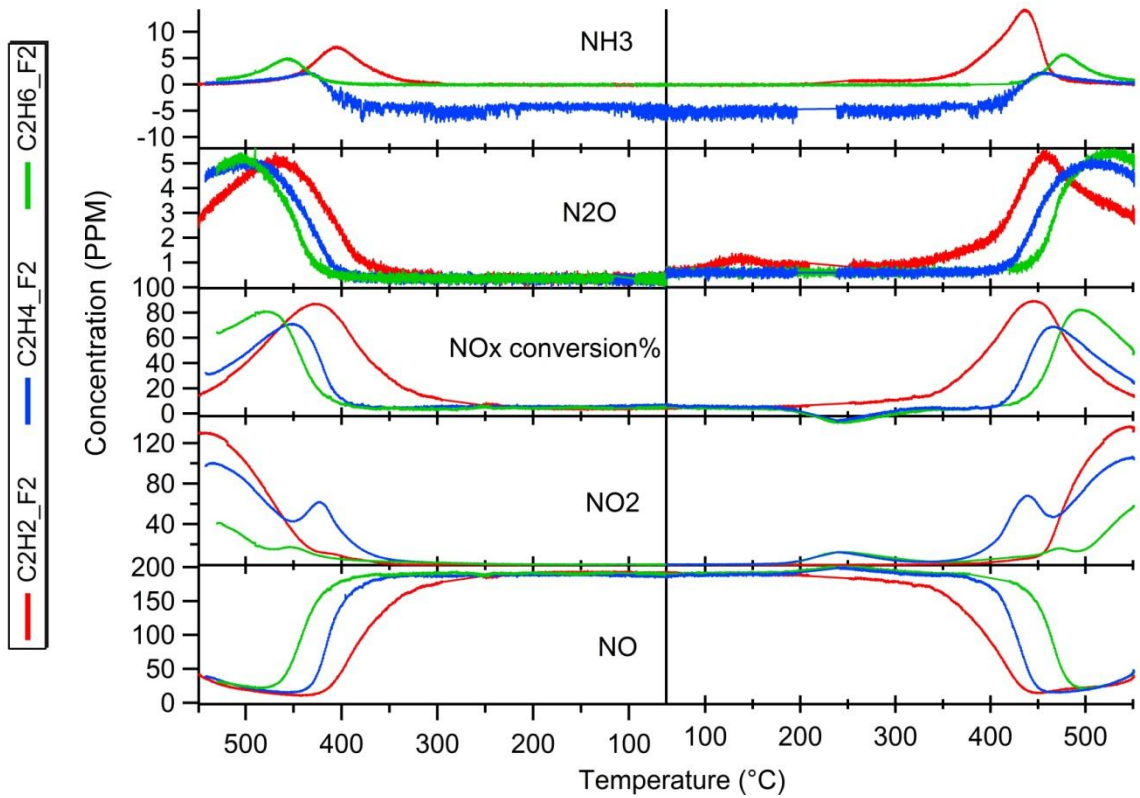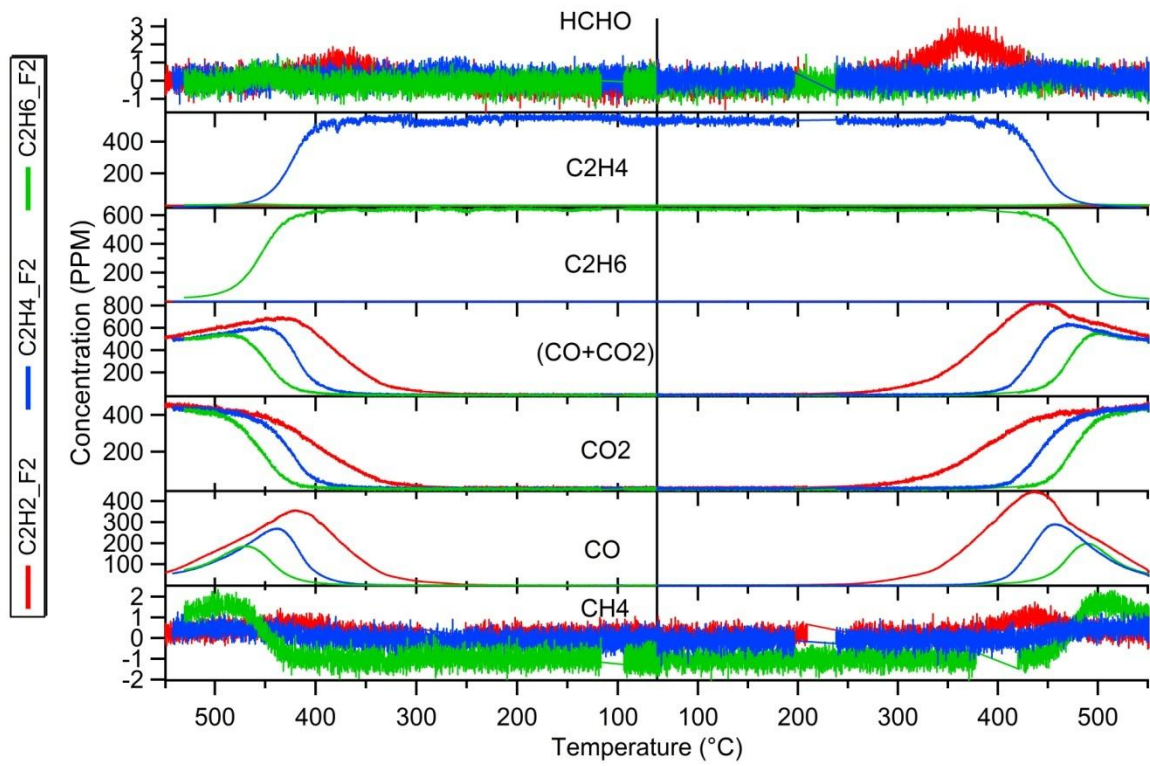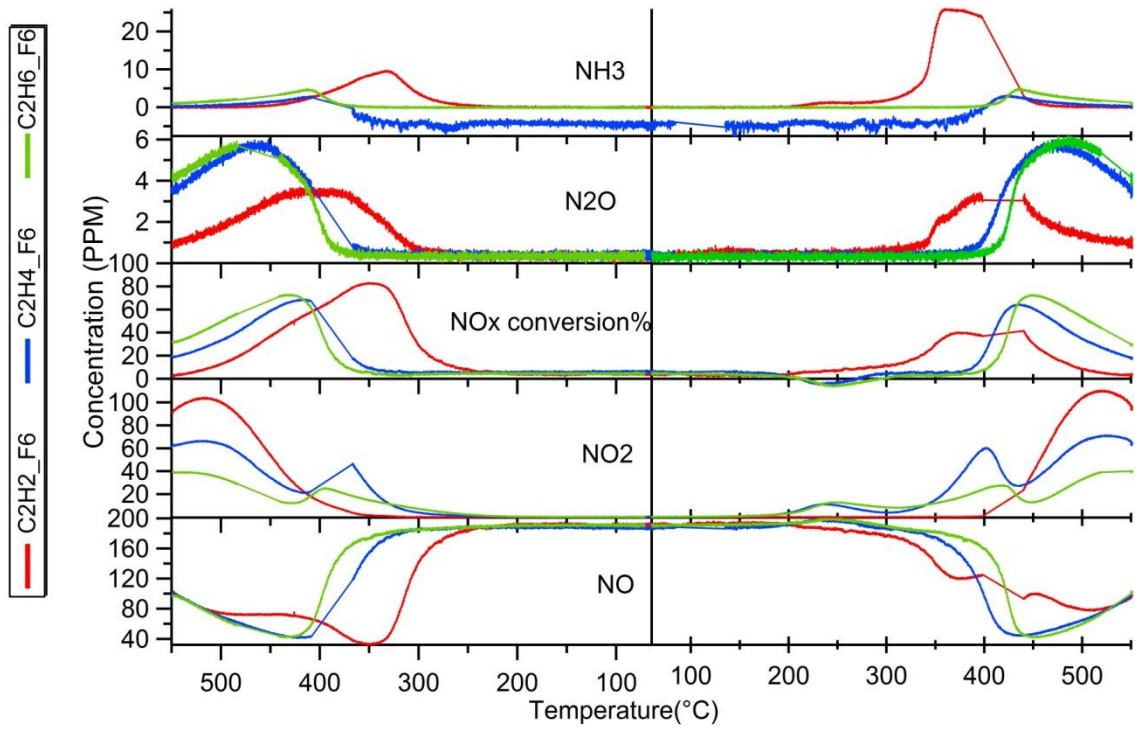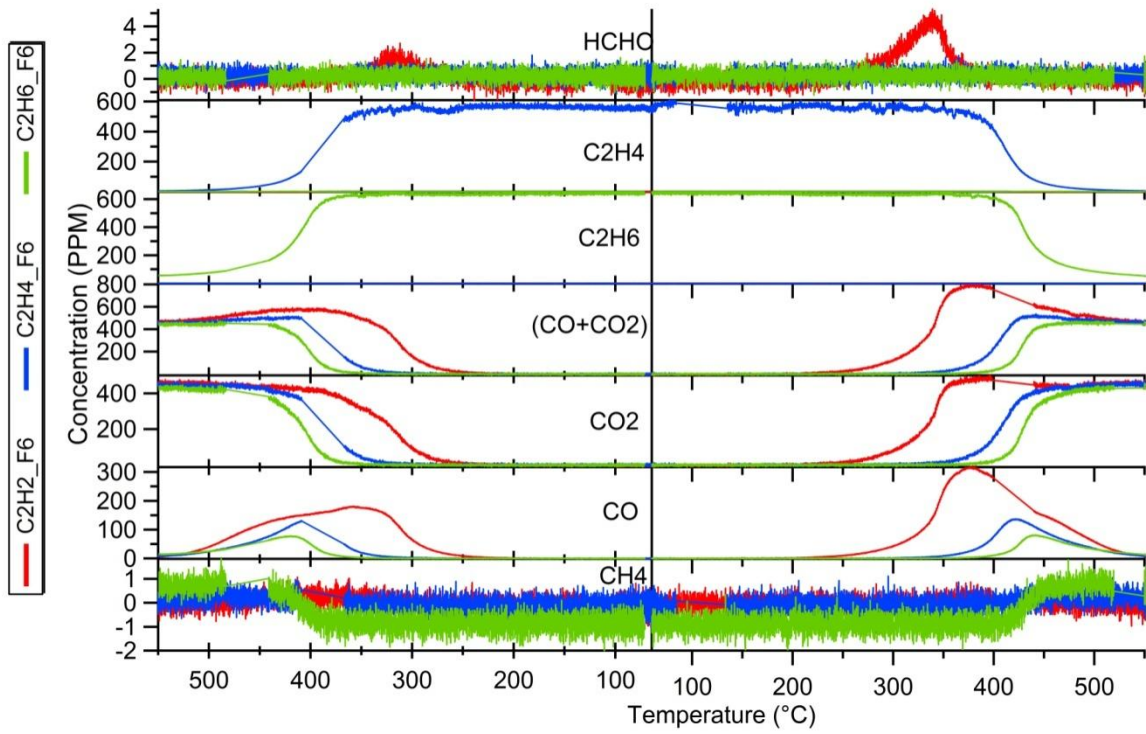
References

[1]   L. Chapman, Journal of transport geography 15 (2007) 354.

[2]   F.M. Viola, S.L.D. Paiva, M.A. Savi, Ecological Modelling 221 (2010) 1964.

[3]   M.A.J. Ed. K.R. Gupta, Klaus Bosselmann, Prasenjit Maiti, Global environment: problems and policies, Atlantic Publishers & Distributors (P) Ltd, New Delhi, 2008.

[4]   P. Barbaro, C. Bianchini, Catalysis for sustainable energy production, Vch Pub, Weinheim, 2009.

[5]   K. Skalska, J.S. Miller, S. Ledakowicz, Science of The Total Environment (2010) 3976.

[6]   R. Burch, Catalysis Reviews 46 (2004) 271.

[7]   J. Mathews, Energy Policy 35 (2007) 4247.

[8]   United Nations framework convention on climate change, 2011-02-23, http://unfccc.int/resource/docs/convkp/conveng.pdf

[9]   D.G. Kessel, Journal of Petroleum Science and Engineering 26 (2000) 157.

[10]   J. Kaspar, P. Fornasiero, N. Hickey, Catalysis Today 77 (2003) 419.

[11]   R. Colvile, E. Hutchinson, R. Warren, Developments in Environmental Sciences 1 (2002) 187.

[12]   I. Chorkendorff, J.W. Niemantsverdriet, Concepts of modern catalysis and kinetics, Wiley-V CH, Weinheim, 2003, p. 377.

[13]   J. Kagawa, Toxicology 181 (2002) 349.

[14]   R.M. Heck, R.J. Farrauto, Applied Catalysis A: General 221 (2001) 443.

[15]   W. Bögner, M. Krämer, B. Krutzsch, S. Pischinger, D. Voigtländer, G. Wenninger, F. Wirbeleit, M. Brogan, R. Brisley, D. Webster, Applied Catalysis B: Environmental 7 (1995) 153.

[16]   K.S. Kabin, R.L. Muncrief, M.P. Harold, Catalysis Today 96 (2004) 79.

[17]   M. Zheng, G.T. Reader, J.G. Hawley, Energy Conversion and Management 45 (2004) 883.

[18]   S. Hodjati, K. Vaezzadeh, C. Petit, V. Pitchon, A. Kiennemann, Catalysis Today 59 (2000) 323.

[19]   N. Takahashi, K. Yamazaki, H. Sobukawa, H. Shinjoh, Applied Catalysis B: Environmental 70 (2007) 198.

[20]   A. Lindholm, N.W. Currier, E. Fridell, A. Yezerets, L. Olsson, Applied Catalysis B: Environmental 75 (2007) 78.

[21]   R.M. Heck, R.J. Farrauto, S.T. Gulati, Catalytic air pollution control: commercial technology, Wiley, New York, 2009, p. 407.

[22]   P.L.T. Gabrielsson, Topics in Catalysis 28 (2004) 177.

[23]   W. Held, A. Koenig, L. Puppe, SAE Technical Papers, 900496, 1990.

[24]   J.H. Baik, S.D. Yim, I.S. Nam, Y.S. Mok, J.H. Lee, B.K. Cho, S.H. Oh, Topics in Catalysis 30 (2004) 37.

[25]   G. Ertl, H. Knözinger, J. Weitkamp, F. Schüth, (1997).

[26] E. Corbos, M. Haneda, X. Courtois, P. Marecot, D. Duprez, H. Hamada, Applied Catalysis A: General 365 (2009) 187.

[27] E. Corbos, M. Haneda, X. Courtois, P. Marecot, D. Duprez, H. Hamada, Catalysis Communications 10 (2008) 137.

[28] M. Iwamoto, H. Hamada, Catalysis Today 10 (1991) 57.

[29] R.J. Farrauto, R.M. Heck, Catalysis Today 51 (1999) 351.

[30] M.D. Amiridis, T. Zhang, R.J. Farrauto, Applied Catalysis B: Environmental 10 (1996) 203.

[31] H. Hamada, Y. Kintaichi, M. Sasaki, T. Ito, M. Tabata, Applied Catalysis 75 (1991) L1.

[32] A. Obuchi, A. Ohi, M. Nakamura, A. Ogata, K. Mizuno, H. Ohuchi, Applied Catalysis B: Environmental 2 (1993) 71.

[33] K. Shimizu, A. Satsuma, T. Hattori, Applied Catalysis B: Environmental 25 (2000) 239.

[34] R. Burch, P. Millington, Catalysis Today 26 (1995) 185.

[35] C.L. DiMaggio, G.B. Fisher, K.M. Rahmoeller, M. Sellnau, SAE International Journal of Fuels and Lubricants 2 (2009) 66.

[36] T. Miyadera, Applied Catalysis B: Environmental 2 (1993) 199.

[37] T. Nakatsuji, R. Yasukawa, K. Tabata, K. Ueda, M. Niwa, Applied Catalysis B: Environmental 17 (1998) 333.

[38] M. Shelef, Chemical Reviews 95 (1995) 209.

[39] S. Satokawa, Chem. Lett. 29 (2000) 294.

[40] J. Breen, R. Burch, Topics in Catalysis 39 (2006) 53.

[41] S. Satokawa, J. Shibata, K. Shimizu, A. Satsuma, T. Hattori, T. Kojima, Chemical Engineering Science 62 (2007) 5335.

[42] M.C. Kung, H.H. Kung, Topics in Catalysis 10 (2000) 21.

[43] X. She, M. Flytzani-Stephanopoulos, Journal of Catalysis 237 (2006) 79.

[44] K. Shimizu, J. Shibata, H. Yoshida, A. Satsuma, T. Hattori, Applied Catalysis B: Environmental 30 (2001) 151.

[45] N. Bogdanchikova, F. Meunier, M. Avalos-Borja, J. Breen, A. Pestryakov, Applied Catalysis B: Environmental 36 (2002) 287.

[46] F. Meunier, J. Breen, V. Zuzaniuk, M. Olsson, J. Ross, Journal of Catalysis 187 (1999) 493.

[47] K. Bethke, H. Kung, Journal of Catalysis 172 (1997) 93.

[48] C. Shi, M. Cheng, Z. Qu, X. Bao, Applied Catalysis B: Environmental 51 (2004) 171.

[49] J. Shibata, Y. Takada, A. Shichi, S. Satokawa, A. Satsuma, T. Hattori, Journal of Catalysis 222 (2004) 368.

[50] K. Shimizu, M. Tsuzuki, K. Kato, S. Yokota, K. Okumura, A. Satsuma, (2006).

[51] M. Campanati, G. Fornasari, A. Vaccari, Catalysis Today 77 (2003) 299.

[52] H. Kannisto, H.H. Ingelsten, M. Skoglundh, Journal of Molecular Catalysis A: Chemical 302 (2009) 86-96.

[53] G. Ertl, H. Knözinger, J. Weitkamp, Preparation of solid catalysts, WILEY-VCH, Weinheim, 1999, pp. 85-89.

[54] A.E.W.B. T. Alexander Nijhuis, Theo Vergunst, Ingrid Hoek, Freek Kapteijn, Jacob A. Moulijn, Catalysis Reviews 43(4) (2001) 345.

[55] C.J. Brinker, G.W. Scherer, Sol-gel science: the physics and chemistry of sol-gel processing, Academic Pr, 1990, p. 2.

[56] K.P. de Jong, Synthesis of solid catalysts, Vch Pub, Weinheim, 2009, p. 194.

[57] J.W. Geus, J.C. Van Giezen, Catalysis Today 47 (1999) 169.

[58] S. Brunauer, P. Emmett, E. Teller, Journal of the American Chemical Society 60 (1938) 309.

[59] M. Bowker, The basis and applications of heterogeneous catalysis, Oxford University Press, 1998, p. 56.

[60] E.P. Barrett, L. Joyner, P. Halenda, Industrial & Engineering Chemistry 44 (1952) 1827.

[61] TRISTAR II 3020, Technique Overview, 2011-02-24, http://www.micromeritics.com/Repository/Files/TRISTAR_II_3020_TECHNIQUE_OVERVIEW.pdf

[62] G. Busca, Catalysis Today 27 (1996) 323.

[63] J. Niemantsverdriet, Spectroscopy in Catalysis, Wiley-VCH, Weinheim, pp. 201-218.

[64] T. Armaroli, T. Bécue, S. Gautier, Oil & Gas Science and Technology 59 (2004) 215.

[65] J.T. Kummer, Prog. Energy Combust. Sci. 6 (1980) 177.

[66] K.C. Taylor, Chem. Tech. 20 (1990) 551.

[67] B.T. B. Djonev, D. Klissurski, K. Hadjiivanov, J. Chem. Soc. Faraday Trans. 93 (1997) 4055.

[68] K. Shimizu, J. Shibata, H. Yoshida, A. Satsuma, T. Hattori, Applied Catalysis B: Environmental 30 (2001) 151-162.

[69] J. Olmsted, G.M. Williams, Chemistry, the molecular science, Jones & Bartlett Pub, Iowa, 1997, p. 413.

[70] P. Siegbahn, Theoretical Chemistry Accounts: Theory, Computation, and Modeling (Theoretica Chimica Acta) 87 (1994) 277.

[71] A.A. Davydov, Infrared Spectroscopy of Adsorbed Species on the Surface of Transition Metal Oxides, John Wiley & Sons, New York, 1990, p. 39.

[72] C. Morterra, G. Magnacca, Catalysis Today 27 (1996) 497.

[73] K. Shimizu, H. Kawabata, A. Satsuma, T. Hattori, J. Phys. Chem. B 103 (1999) 5240.

[74] N. Bion, J. Saussey, M. Haneda, M. Daturi, Journal of Catalysis 217 (2003) 47.

[75] Y. Yu, X. Zhang, H. He, Applied Catalysis B: Environmental 75 (2007) 298.

[76] H. He, C. Zhang, Y. Yu, Catalysis Today 90 (2004) 191.

[77] A. Satsuma, K. Shimizu, Progress in Energy and Combustion Science 29 (2003) 71.

[78] F. Meunier, V. Zuzaniuk, J. Breen, M. Olsson, J. Ross, Catalysis Today 59 (2000) 287.

[79] T. Chafik, S. Kameoka, Y. Ukisu, T. Miyadera, Journal of Molecular Catalysis A: Chemical 136 (1998) 203.

[80] Z. Liu, S.I. Woo, W.S. Lee, J. Phys. Chem. B 110 (2006) 26019.

[81] Y. Yu, H. He, Q. Feng, H. Gao, X. Yang, Applied Catalysis B: Environmental 49 (2004) 159.

[82] S. Kameoka, Y. Ukisu, T. Miyadera, PCCP. Physical chemistry chemical physics 2 (2000) 367.

[83] H.H. Ingelsten, A. Hellman, H. Kannisto, H. Grönbeck, Journal of Molecular Catalysis A: Chemical 314 (2009) 102.

[84] K.I. Hadjiivanov, Catal. Rev. Sci. Eng. 42 (2000) 71.

[85] A. Iglesias-Juez, A. Hungria, A. Martínez-Arias, A. Fuerte, M. Fernandez-Garcia, J. Anderson, J. Conesa, J. Soria, Journal of Catalysis 217 (2003) 310.

[86] S. Tamm, H.H. Ingelsten, A.E.C. Palmqvist, Journal of Catalysis 255 (2008) 304.

[87] V. Zuzaniuk, F.C. Meunier, J.R.H. Ross, Journal of Catalysis 202 (2001) 340.